

A Policy Optimization Method Towards Optimal-time Stability

Anonymous Author(s)

Affiliation

Address

email

Abstract: In current model-free reinforcement learning (RL) algorithms, stability criteria based on sampling methods are commonly utilized to guide policy optimization. However, these criteria only guarantee the infinite-time convergence of the system’s state to an equilibrium point, which leads to sub-optimality of the policy. In this paper, we propose a policy optimization technique incorporating sampling-based Lyapunov stability. Our approach enables the system’s state to reach an equilibrium point within an optimal time and maintain stability thereafter, referred to as "*optimal-time stability*". To achieve this, we integrate the optimization method into the Actor-Critic framework, resulting in the development of the Adaptive Lyapunov-based Actor-Critic (ALAC) algorithm. Through evaluations conducted on ten robotic tasks, our approach outperforms previous studies significantly, effectively guiding the system to generate stable patterns.

Keywords: Reinforcement Learning, Robotic Control, Stability

1 Introduction

Model-free reinforcement learning (RL) controllers have achieved excellent performance in a large variety of robotic tasks [1, 2]. However, current methods lack a stability guarantee, which poses additional risks to both the robots and their environments, especially in the presence of external disturbances [3]. Therefore, ensuring stability in RL-based methods is a crucial requirement.

In control-theoretic methods, there exists an effective tool, Lyapunov functions, to assess the stability [4]. Recently, researchers have employed neural networks to search for feasible Lyapunov functions [5, 6, 7, 8]. Notably, model-free methods have integrated policy and Lyapunov function learning based on discrete sampling-based stability, demonstrating promising results in robotic control tasks [9, 10, 11, 12, 13] (See Appendix A for related work). However, these methods only guarantee the eventual convergence of the system’s state

to an equilibrium point. Figure 1 illustrates a limitation of this guarantee, where two stability-maintaining state trajectories (colored cyan and purple) cannot be differentiated by current methods, despite the purple trajectory exhibiting better stability convergence efficiency. In our experiments,

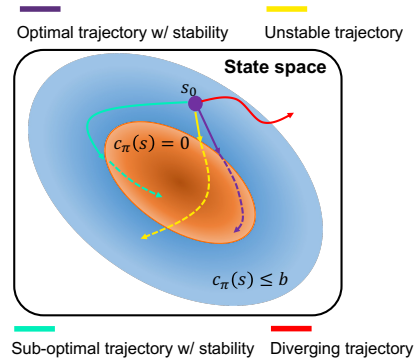


Figure 1: Intuitive example showing the optimality and stability. The stability condition is the mean cost stability defined in Definition 2.1. The figure shows the relationship between three sets, like the whole state space, $\{s \mid c_\pi(s) \leq b\}$ and $\{s \mid c_\pi(s) = 0\}$. The red line represents a diverging trajectory. The yellow line represents a trajectory without stability. The trajectories coloured cyan and purple remain stable, whereas the state in the purple trajectory reaches the set $\{s \mid c_\pi(s) = 0\}$ more quickly.

we find that this loose guarantee fails to provide adequate guidance for policy learning. Inspired by finite-time stability in continuous-time control theory [14], we propose an improved objective where the state converges to the equilibrium point within an optimal time, which we refer to as "*optimal-time stability*" in this paper. This optimal condition facilitates rapid convergence to the equilibrium point while ensuring stability in the system. Our objective is to develop a policy capable of generating the purple trajectory depicted in Figure 1.

To ensure *optimal-time stability* in the system, we introduce a sampling-based Lyapunov stability certification, which guarantees the fulfillment of the mean cost stability condition. Subsequently, we design a policy optimization method that facilitates the gradual convergence of the policy towards the optimal point, where the system achieves *optimal-time stability*. By leveraging this policy optimization technique, we develop the Adaptive Lyapunov-based Actor-Critic algorithm (ALAC) for learning both a Lyapunov function and policy. Experimental results validate the effectiveness of our approach in ensuring optimality and stability across various robotic control tasks, including legged robot walking and free-floating space robot trajectory planning. Specifically, our method significantly outperforms baselines in ten robotic control environments, and the trained Lyapunov function provides effective guidance for policy learning compared to previous methods¹.

2 Problem Formulation

A robotic system can be modelled as a Markov Decision Process (MDP). MDP mainly consists of five elements, \mathcal{S} , \mathcal{A} , \mathcal{P} , \mathcal{C} and ρ . Here, \mathcal{S} is the state space, \mathcal{A} is the action space, \mathcal{P} is the dynamic transition function, and \mathcal{C} is the cost function. Besides, the distribution of starting state denotes $s_0 \sim \rho$. At timestep t , $s_t \in \mathcal{S}$ represents the state the robot observes. Then, $a_t \in \mathcal{A}$ is the action executed by the agent (robot). Note that a_t is sampled from the agent's policy $\pi(a_t|s_t)$. According to $\mathcal{P}(s_{t+1}|s_t, a_t)$, the state of system transfers to the next state s_{t+1} with a certain probability. At the same time, the agent receives the cost $\mathcal{C}(s_t, a_t)$. And then, we can define the state distribution \mathcal{T} :

$$\mathcal{T}(s|\rho, \pi, t+1) = \int_{\mathcal{S}} \int_{\mathcal{A}} \pi(a_t|s_t) \mathcal{P}(s_{t+1}|s_t, a_t) da \mathcal{T}(s|\rho, \pi, t) ds \quad (1)$$

Note that $\mathcal{T}(s|\rho, \pi, 0) = \rho$ holds.

An MDP system corresponds to a continuous-state and discrete-time dynamical system with state space \mathcal{S} and action space \mathcal{A} . Generally speaking, the system's stability can be verified by a classical tool, Lyapunov's stability function (Appendix B.1). However, the classical definition should be satisfied in the whole state space \mathcal{S} , so it is unsuitable for sampling optimization, especially for model-free RL methods. To extend the stability to a reasonable case in model-free RL, we introduce the Mean Cost Stability as the stability condition in this paper.

Definition 2.1 (Mean Cost Stability). A robotic system remains stable in mean cost when satisfying the following equation, where $c_\pi(s_t) = \mathbb{E}_{a \sim \pi} \mathcal{C}(s_t, a_t)$ and b is a constant [9].

$$\lim_{t \rightarrow \infty} \mathbb{E}_{s_t \sim \mathcal{T}} c_\pi(s_t) = 0, c_\pi(s_0) \leq b \quad (2)$$

Concretely, for most robotic tasks, the mean cost stability is related to the stability of the closed-loop system [9]. Our aim is to reach an equilibrium point within an optimal time and behave stably around it, to achieve the *optimal-time stability*. Thus, we construct the problem formulation represented as follows:

$$\min_{\pi} \mathbb{E}_{\rho, \pi, \mathcal{P}} \left[\sum_{t=0}^{\infty} \gamma^t c_\pi(s_t) \right] \quad s.t. \quad \lim_{t \rightarrow \infty} \mathbb{E}_{s_t \sim \mathcal{T}} c_\pi(s_t) = 0 \quad (3)$$

Specifically, the constraint part can facilitate the system's state to converge to an equilibrium point. The objective of the task is to minimize the sum of discounted costs. When the sum of discounted costs becomes smaller, the system converges to an equilibrium point more quickly. Therefore, by minimizing the sum of discounted costs, we ensure that the system's state converges to an equilibrium point within an optimal time.

¹For more information, please visit our project page at <https://sites.google.com/view/adaptive-lyapunov-actor-critic>.

81 3 Policy Optimization with Sampling-based Stability

82 First, we present a sampling-based Lyapunov stability certification that satisfies the mean cost stability
 83 condition defined in Definition 2.1. Additionally, we introduce a Lyapunov candidate and learnable
 84 parameters into the stability condition, to design a policy optimization method for the problem (3).

85 3.1 Sampling-based Stability Certification

86 The sampling-based Lyapunov stability we propose is based on some mild assumptions as shown
 87 in Appendix C.1. Furthermore, we define the sampling distribution $\mathcal{U}_\pi = \lim_{T \rightarrow \infty} \frac{1}{T} \sum_{t=0}^T \mathcal{T}(s |$
 88 $\rho, \pi, t)$. Then, the sampling-based Lyapunov stability is given over the sample distribution \mathcal{U}_π .

89 **Theorem 3.1** (Sampling-based Lyapunov Stability). *An MDP system is stable with regard to the*
 90 *mean cost as shown in Definition 2.1, if there exists a function $\mathcal{L} : S \rightarrow \mathbb{R}$ meets the following*
 91 *conditions:*

$$92 \quad \alpha c_\pi(s) \leq \mathcal{L}(s) \leq \beta c_\pi(s) \quad (4)$$

$$93 \quad \mathcal{L}(s) \geq c_\pi(s) + \lambda \mathbb{E}_{s' \sim \mathcal{P}_\pi} \mathcal{L}(s') \quad (5)$$

$$94 \quad \mathbb{E}_{s \sim \mathcal{U}_\pi} [\mathbb{E}_{s' \sim \mathcal{P}_\pi} \mathcal{L}(s') - \mathcal{L}(s)] \leq -k [\mathbb{E}_{s \sim \mathcal{U}_\pi} [\mathcal{L}(s) - \lambda \mathbb{E}_{s' \sim \mathcal{P}_\pi} \mathcal{L}(s')]] \quad (6)$$

94 where α, β, λ and k is positive constants. Among them, $\mathcal{P}_\pi(s'|s) = \int_{\mathcal{A}} \pi(a|s) \mathcal{P}(s'|s, a) da$ holds.
 95 For proof, please see Appendix C.2.

96 In practice, the theorem reveals that the guarantee of sampling-based Lyapunov stability corresponds
 97 to the existence of \mathcal{L} function. It is worth noting that our method extends the previous method to a more
 98 general case. Intuitively, the previous method is a special case when $\mathcal{L}(s) = c_\pi(s) + \lambda \mathbb{E}_{s' \sim \mathcal{P}_\pi} \mathcal{L}(s')$
 99 holds [9]. Taking advantage of the sampling-based Lyapunov stability, we can obtain the policy that
 100 guarantees the system's stability in the RL framework.

101 3.2 Policy Optimization Towards Optimal-time Stability

102 To mitigate the searching difficulty under multiple constraints, we propose a Lyapunov can-
 103 didate $\mathcal{L}_\pi(s)$ which naturally meets the constraints in Equation (4) and (5), $\mathcal{L}_\pi(s) =$
 104 $\mathbb{E}_\pi[\sum_{t=0}^{\infty} \gamma^t c_\pi(s_t) | s_0 = s]$. Please see Appendix B.2 for a detailed demonstration. Recalling the
 105 optimization problem (3), we find that the constraint part equals Equation (6) with respect to $\mathcal{L}_\pi(s)$,
 106 as well as the objective part can be represented as $\min_\pi \mathbb{E}_{s \sim \rho} \mathcal{L}_\pi(s)$. Therefore, the optimization
 107 problem can be rewritten as:

$$108 \quad \begin{aligned} & \min_{\pi} \mathbb{E}_{s \sim \rho} \mathcal{L}_\pi(s) \\ & \text{s.t. } \mathbb{E}_{s \sim \mathcal{U}_\pi} [\mathbb{E}_{s' \sim \mathcal{P}_\pi} \mathcal{L}_\pi(s') - \mathcal{L}_\pi(s)] \leq -k [\mathbb{E}_{s \sim \mathcal{U}_\pi} [\mathcal{L}_\pi(s) - \lambda \mathbb{E}_{s' \sim \mathcal{P}_\pi} \mathcal{L}_\pi(s')]] \end{aligned} \quad (7)$$

108 A potential approach to tackle the problem (7) is to formulate a unified objective function that removes
 109 the constraints. However, directly combining the objective with constraints through simple addition
 110 may lead to a sub-optimal policy or an invalid Lyapunov function. Therefore, we propose a policy
 111 optimization method that progressively seeks the optimal policy while ensuring stability by making
 112 the constraints' parameters λ and k learnable. The method is outlined as follows.

$$113 \quad \max_{\lambda, k} \mathbb{E}_{s \sim \mathcal{U}_\pi} \Delta \mathcal{L}_\pi(s) \quad \text{s.t. } \pi \in \{\pi | \mathbb{E}_{s \sim \mathcal{U}_\pi} \Delta \mathcal{L}_\pi(s) \leq 0\} \quad (8)$$

113 where

$$114 \quad \Delta \mathcal{L}_\pi(s) = \mathbb{E}_{s' \sim \mathcal{P}_\pi} \mathcal{L}_\pi(s') - \mathcal{L}_\pi(s) + k [\mathcal{L}_\pi(s) - \lambda \mathbb{E}_{s' \sim \mathcal{P}_\pi} \mathcal{L}_\pi(s')] \leq 0 \quad (9)$$

114 Intuitively, the constraint part corresponds to the constraints defined in Equation (7). The objective
 115 seeks to find optimal values for λ and k to maximize $\mathbb{E}_{s \sim \mathcal{U}_\pi} \Delta \mathcal{L}_\pi(s)$. Alternatively, we can view this
 116 objective as enhancing the strength of the constraints by maximizing $\mathbb{E}_{s \sim \mathcal{U}_\pi} \Delta \mathcal{L}_\pi(s)$. By gradually
 117 improving the constraints, minimizing $\mathcal{L}_\pi(s)$ can be achieved in Equation (7). Because, as the
 118 constraints improve, the policy should ensure that $\mathcal{L}_\pi(s')$ at the next state becomes smaller, as

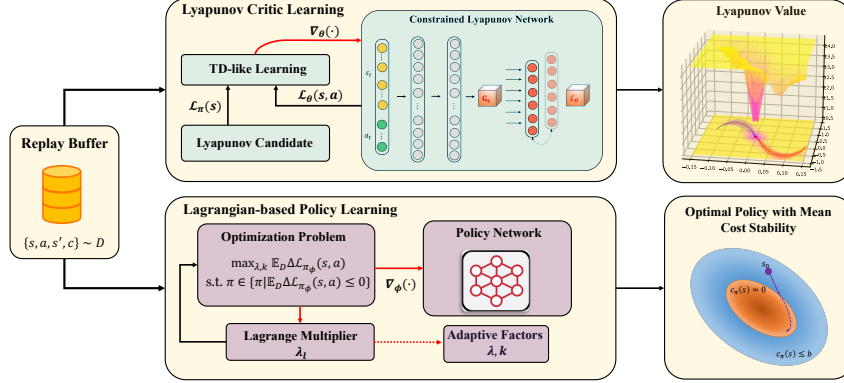


Figure 2: Architecture illustrating the practical implementation of ALAC. The RL agent is optimized by an Actor-Critic framework. The main contents consist of two parts. For the Lyapunov critic learning, the constrained Lyapunov network is updated by the TD-like learning with respect to the Lyapunov candidate. During the policy Learning, we use the Lagrangian-based method to solve the optimization problem shown in Equation (8). Meanwhile, the parameters λ and k are adjusted by the Lagrange multiplier λ_l adaptively.

119 dictated by the constraint part in Equation (8). Considering the sampling distribution \mathcal{U}_π , \mathcal{L}_π becomes
 120 simultaneously smaller at every state along the state trajectories. This also applies to \mathcal{L}_π under
 121 the initial state distribution ρ . As the strength of the constraints reaches its maximum value, the
 122 minimization of $\mathcal{L}_\pi(s)$ is achieved. Furthermore, Equation (8) decouples the learning of policy and
 123 constraints' parameters to simplify the complexity of the problem.

124 In addition, we offer a comprehensive illustration to explain the decrease of $\mathcal{L}_\pi(s')$ using a classical
 125 tracking task, which is provided in Appendix C.4. Interestingly, the form of Equation (9) bears
 126 resemblance to the finite-time tracking method in continuous-time systems (Appendix C.3).

127 4 Adaptive Lyapunov-based Actor-Critic Algorithm

128 In this section, we propose the Adaptive Lyapunov-based Actor-Critic algorithm (ALAC) to solve the
 129 problem shown in Equation (8). The main contents are as follows: 1) we construct an Actor-Critic
 130 framework that facilitates the learning of both the Lyapunov function and the policy; 2) we use a
 131 TD-like learning method to update the parameters of the constrained Lyapunov network; 3) we apply
 132 the Lagrangian-based method to realize the process of policy optimization. Concretely, Figure 2
 133 shows the architecture of the ALAC algorithm.

134 First, we construct two neural networks, namely actor $\pi_\phi(a|s)$ and Lyapunov critic $\mathcal{L}_\theta(s, a)$. Among
 135 them, ϕ and θ represent the parameters of two networks, respectively. The actor $\pi_\phi(a|s)$ maps a
 136 given state s to a distribution over action. The action distribution is modelled as a Gaussian, with a
 137 state-dependent mean $\mu_\phi(s)$ and diagonal covariance matrix $\Sigma_\phi(s)$.

138 4.1 Lyapunov Critic Learning

139 The learning of Lyapunov critic $\mathcal{L}_\theta(s, a)$ aims to fit the value of the target Lyapunov candidate $\mathcal{L}_\pi(s)$.
 140 As a matter of fact, $\mathcal{L}_\pi(s)$ is the expectation of $\mathcal{L}_\theta(s, a)$ over the distribution of actions. Specifically,
 141 $\mathbb{E}_\pi \mathcal{L}_\theta(s, a) = \mathcal{L}_\pi(s)$ holds. In the context of this property, the above theoretical results about $\mathcal{L}_\pi(s)$
 142 are also suitable for our critic network.

143 For the training of $\mathcal{L}_\theta(s, a)$, because we choose the value function as the Lyapunov candidate, we
 144 can update θ according to the TD error:

$$\theta_{k+1} = \theta_k + \alpha_\theta (\nabla_\theta (\mathcal{L}_\theta(s, a) - (c_\pi + \gamma \mathcal{L}'(s', \pi'(\cdot|s'))))^2) \quad (10)$$

145 where k is the number of iterations. \mathcal{L}' and π' are the target networks parameterized by θ' and
 146 ϕ' , respectively. In the Actor-Critic method, the parameters θ' and ϕ' are usually updated through

147 exponentially moving average of weights controlled by a hyper-parameter $\sigma \in (0, 1)$. In order to
 148 encourage accurate and efficient learning, we construct a constrained critic network. The constrained
 149 network ensures that the output is non-negative and the Lyapunov value should be zero when the state
 150 is an equilibrium point. For the details, please see Appendix C.5.

151 4.2 Lagrangian-based Policy Learning

152 Policy learning aims to search feasible parameters of λ , k and the policy network to solve the
 153 optimization problem defined in Equation (8). According to Equation (9), we denote $\Delta\mathcal{L}_{\pi_\phi}(s, a)$ as
 154 $\mathcal{L}_\theta(s', \pi_\phi(\cdot | s')) - \mathcal{L}_\theta(s, a) + k[\mathcal{L}_\theta(s, a) - \lambda\mathcal{L}_\theta(s', \pi_\phi(\cdot | s'))]$.

155 First, we solve the sub-problem of Equation (8), finding π_ϕ when satisfying the constraint with
 156 arbitrary λ . Applying the Lagrangian-based method [15], the parameters of π_ϕ are updated by:

$$\phi_{k+1} = \phi_k + \alpha_\phi(\lambda_l \nabla_a \Delta\mathcal{L}_{\pi_\phi}(s, a) \nabla_\phi \pi_\phi(s, a)) \quad (11)$$

157 where α_ϕ is the learning rate of ϕ . λ_l represents the Lagrange multiplier of the constraint. During the
 158 training, λ_l is updated by gradient ascent to maximize $\Delta\mathcal{L}_{\pi_\phi}(s, a)$.

$$\lambda_l^{k+1} = \lambda_l^k + \alpha_{\lambda_l} \Delta\mathcal{L}_{\pi_\phi}(s, a) \quad (12)$$

159 Note that λ_l should always be positive. α_{λ_l} is the learning rate. It is worth noting that λ_l is clipped
 160 by 0 and 1, to bound the value.

161 In Section 3.2, we discuss the need to find suitable values for λ and k to maximize $\Delta\mathcal{L}_{\pi_\phi}(s, a)$ and
 162 enhance the constraints. Referring to Equation (9), we observe that λ should decrease towards 0 to
 163 improve the constraints. Meanwhile, we find the Lagrange multiplier λ_l ranging from 1 to 0, where
 164 it decreases as the constraints are satisfied. To update λ , we use the rule $\lambda \leftarrow \min(\lambda_l, \gamma)$, with the
 165 range of λ restricted based on Theorem 3.1, where it should be between γ and 0. As for the selection
 166 of k , we adjust its value based on the Lagrange multiplier, setting $k \leftarrow 1 - \lambda_l$. By increasing k , the
 167 strength of the constraints gradually improves throughout the training process. Finally, when λ and k
 168 stabilize, indicating that the Lagrange multiplier λ_l remains constant, we can observe that $\Delta\mathcal{L}_{\pi_\phi}(s, a)$
 169 approaches 0 according to Equation (12). This implies that the objective of maximizing $\Delta\mathcal{L}_{\pi_\phi}(s, a)$
 170 is achieved since the maximum value of $\Delta\mathcal{L}_{\pi_\phi}(s, a)$ does not exceed 0 due to the constraint part
 171 in Equation (8). Besides, the updating of k and λ has the corresponding effect on the strength of
 172 constraints, so it doesn't cause the training collapse.

173 In addition, to improve the exploration efficiency, we add a constraint about the minimum entropy as
 174 the same as the maximum entropy RL algorithms. Until now, we have designed the complete ALAC
 175 algorithm, and the pseudo-code is provided in Appendix D.

176 4.3 Theoretical Analysis

177 Theorem 3.1 has assumed that the expectation is obtained perfectly, but this is not the case in practical
 178 settings due to finite samplings. Thus, we derive the bias between the practical computing and
 179 theoretical analysis about \mathcal{U}_π .

180 To be concrete, we need an infinite number of trajectories with infinite time steps to estimate
 181 the distribution \mathcal{U}_π . Whereas in practice, only M trajectories of T time steps are accessible. To
 182 better illustrate the issue, we define a finite sampling distribution \mathcal{U}_π^T , apparently where $\mathcal{U}_\pi^T =$
 183 $\frac{1}{T} \sum_{t=0}^T \mathcal{T}(s | \rho, \pi, t)$. First, we provide a quantitative bound of expectation from \mathcal{U}_π and \mathcal{U}_π^T .

184 **Theorem 4.1.** *Suppose that the length of sampling trajectories is T , then the bound can be expressed*
 185 *as:*

$$|\mathbb{E}_{s \sim \mathcal{U}_\pi} \Delta\mathcal{L}_\pi(s) - \mathbb{E}_{s \sim \mathcal{U}_\pi^T} \Delta\mathcal{L}_\pi(s)| \leq 2 \frac{(k+1)\bar{c}_\pi}{1-\gamma} T^{q-1} \quad (13)$$

186 where \bar{c}_π is the maximum of cost and q is a constant in $(0, 1)$. For proof, please see Appendix C.6.

187 Next, we take the number of trajectories into consideration and derive the probabilistic bound of the
 188 difference of $\Delta\mathcal{L}_\pi(s)$ estimated by \mathcal{U}_π^T distribution and M trajectories.

Table 1: Performance evaluations of the cultivated costs and stability constraint violations on ten environments compared with six baselines. All quantities are provided in a scale of 0.1. Standard errors are provided in brackets. (if the mean constraint violations are less than 0.2, the sign is ↓ else ↑. ‘-’ indicates the algorithm does not contain the stability constraints.)

Task	Metrics	ALAC	SAC-cost	SPPO	LAC	LAC*	POLYC	LBPO	TNLF
Cartpole-cost	Cost Return	26.2(7.0)	22.7 (12.6)	102.3(59.3)	31.0(10.1)	31.5(5.1)	104.8(70.7)	205.3(27.0)	33.5(24.5)
	Violation	↓	-	↑	↓	↓	↓	-	↓
Point-circle-cost	Cost Return	111.1 (4.5)	111.8(2.4)	247.9(58.2)	958.6(15.5)	112.0(5.0)	207.0(62.4)	722.1(126.1)	145.8(38.0)
	Violation	↓	-	↑	↓	↑	↓	-	↓
Halfcheetah-cost	Cost Return	1.7 (0.7)	16.6(25.2)	144.0(14.6)	119.5(37.3)	1.8(0.5)	168.8(10.7)	37.8(24.8)	6.5(1.4)
	Violation	↓	-	↑	↓	↓	↓	-	↓
Swimmer-cost	Cost Return	44.6 (4.8)	53.7(12.4)	52.5(4.2)	47.5(1.3)	44.8(3.0)	104.7(11.0)	52.3(11.3)	46.5(2.4)
	Violation	↓	-	↑	↓	↑	↓	-	↓
Ant-cost	Cost Return	101.0 (42.1)	155.2(29.9)	255.0(31.2)	166.9(13.6)	125.6(12.5)	259.8(37.1)	114.6(26.1)	186.8(11.0)
	Violation	↓	-	↑	↓	↑	↓	-	↓
Humanoid-cost	Cost Return	354.6(97.1)	441.9(18.3)	531.8(22.9)	431.3(14.9)	368.3(76.6)	490.4(32.5)	452.4(13.9)	317.7 (31.1)
	Violation	↓	-	↑	↓	↑	↓	-	↓
Minitaur-cost	Cost Return	493.0(67.9)	692.2(93.0)	950.0(72.3)	612.2(47.8)	666.6(306.7)	608.3(65.6)	838.3(237.0)	382.9 (62.6)
	Violation	↓	-	↑	↓	↑	↓	-	↓
Spacereach-cost	Cost Return	1.6 (0.2)	8.9(8.8)	19.4(2.5)	35.2(1.6)	1.8(0.4)	125.7(20.8)	31.0(19.1)	112.1(53.0)
	Violation	↓	-	↓	↓	↓	↓	-	↓
Spacerandom-cost	Cost Return	2.3 (0.3)	38.4(28.6)	53.2(32.7)	33.9(3.5)	2.8(0.9)	112.8(19.4)	35.8(2.9)	85.9(42.3)
	Violation	↓	-	↓	↓	↓	↓	-	↓
Spacedualarm-cost	Cost Return	26.1 (3.5)	36.1(8.3)	201.9(48.8)	66.3(10.6)	63.6(62.1)	140.6(17.4)	37.8(7.5)	280.1(99.3)
	Violation	↓	-	↓	↓	↓	↓	-	↓

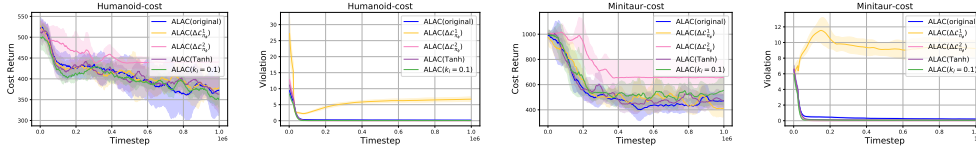


Figure 3: Ablation studies of the sampling-base stability we propose. ALAC(original) shows comparable or the best performance compared with other certifications on each task.

189 **Theorem 4.2.** Suppose that the length of sampling trajectories is T and the number of trajectories is
190 M , then there exists the following upper bound:

$$\mathbb{P}\left(\frac{1}{MT} \sum_{m=1}^M \sum_{t=1}^T \Delta \mathcal{L}_\pi(s_t^m) - \mathbb{E}_{s \sim \mathcal{U}_\pi^T} \Delta \mathcal{L}_\pi(s) \geq \alpha\right) \leq 2 \exp\left(-\frac{M\alpha^2(1-\gamma)^2}{((1-k\lambda)^2 + (k-1)^2)c_\pi^2}\right) \quad (14)$$

191 where s_t^m represents the state in the m -th trajectory at the time t . For proof, please see Appendix C.7.

192 Theorems 4.1 and 4.2 highlight the theoretical gap between infinite and finite samples in practical
193 usage. In addition, they provide valuable insights into the choice of k . Theorem 4.1 suggests that
194 when k approaches 0, the gap becomes small in practice. On the other hand, Theorem 4.2 indicates
195 that k is better to be set to 1. This implies that the optimal choice of k lies within the range of 0 to 1.

196 5 Experiments

197 In this section, we demonstrate empirical evidence that **ALAC** captures an improved trade-off between
198 optimality (sum of costs) and stability compared to the baseline approaches. We test our method and
199 baselines in ten robotic control environments. Details of the environments are given in Appendix
200 E.1. Furthermore, we benchmark the **ALAC** method against five algorithms with a neural Lyapunov
201 function, including **POLYC** [10], **LBPO**[16], **TNLF**[11], **SPPO**[17] and **LAC** [9]². We also take

²We find **LAC** with a large α_3 (see Appendix E.2.1) performs better, so we call it **LAC*** for the distinction between them.

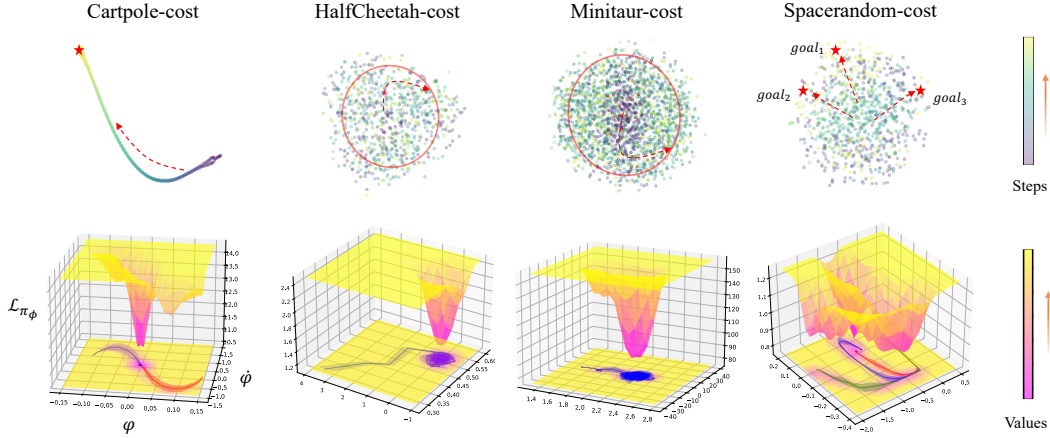


Figure 4: Visualization of states for ALAC method by t-SNE and phase trajectory techniques. The top row of the figure depicts the t-SNE dimension reduction technique. (**Cartpole-Cost** is visualized within 2 dims while others within 3 dims.) The bottom row shows the phase trajectories and Lyapunov-value surfaces of environments. ψ and $\dot{\psi}$ denotes the angular position and velocity respectively.

Table 2: Average evaluation score and standard deviation on our environments for ALAC with and without the errors under different biases of goals. (w/ errors means using errors between the desired and achieved goals as extra elements of states for the agent)

Task Biases of goals	Point-circle-cost			Halfcheetah-cost			Spacereach-cost		
	-20%	0%	20%	-20%	0%	20%	-20%	0%	20%
ALAC w/ errors	85.2(4.5)	110.1(3.9)	148.5(12.2)	3.9 (0.8)	2.5 (0.6)	8.3 (4.7)	6.4 (1.7)	2.4(1.4)	8.7 (1.7)
ALAC w/o errors	178.8(7.8)	118.9(11.4)	247.8(11.9)	10.1(2.1)	3.3(1.2)	13.4(2.1)	11.9(0.4)	1.6 (0.2)	11.5(0.3)
SAC-cost w/ errors	84.2 (4.2)	109.3 (2.2)	140.1 (3.0)	60.1(27.5)	81.6(50.2)	129.5(85.6)	21.9(12.3)	22.1(16.9)	20.6(18.1)
SAC-cost w/o errors	180.9(6.3)	115.3(4.0)	240.3(3.7)	15.9(15.7)	16.7(25.5)	33.5(34.0)	16.1(6.2)	8.8(8.8)	15.0(7.2)

202 the **SAC-cost** [18] method into account because the method is very close to our method without the
 203 stability condition. For the detailed hyper-parameter settings see Appendix E.2.1 and E.2.2.

204 5.1 Comparing with Baselines

205 In this part, we evaluate the optimality and stability of our methods and baselines. The results
 206 demonstrate **ALAC** using *optimal-time stability* makes the system’s state converge to an equilibrium
 207 point within an optimal time compared with baselines. To fairly evaluate the performance of the
 208 methods mentioned above, we run the experiments over 5 rollouts and 5 seeds for all algorithms. We
 209 use the accumulated cost in a testing episode as the metric of optimality and the stability constraint
 210 violations as the stability metric. Table 1 shows the performance on all tasks, and the training curves
 211 for different algorithms are in Appendix E.3. Although **LAC*** using tighter constraints achieves
 212 comparable performance with our method in contrast to **LAC**, the stability violations in **LAC*** remain
 213 at a high level on many tasks. Admittedly, **TNLF** achieves lower cost than **ALAC** on **Minitaur-cost**,
 214 but **TNLF** converges to suboptimal policies on many tasks. According to Figure 10, we notice that in
 215 **TNLF** the trained Lyapunov function is close to 0 quickly. Hence, it does not provide dense guidance
 216 for the policy, thus leading it to a suboptimal solution.

217 5.2 Ablation Studies

218 To demonstrate the effectiveness of $\Delta\mathcal{L}_{\pi_\phi} \leq 0$, we do the ablation studies about different constraints
 219 in **ALAC**. We compare the performance of the original **ALAC** with a version that uses $\Delta\mathcal{L}_{\pi_\phi}^1$
 220 ($\lambda = 0$) and $\Delta\mathcal{L}_{\pi_\phi}^2$ ($\lambda = 1$), and with a version where k is a constant throughout training. The

221 details are given in Appendix E.4. Figure 3 and Figure 9 (see Appendix D.4) depict the accumulated
 222 cost and constraint violations on all tasks, where the algorithms are modified from **ALAC** directly.
 223 **ALAC**($\Delta\mathcal{L}_{\pi_\phi}^2$) achieve lower performance than **ALAC**, while **ALAC**($\Delta\mathcal{L}_{\pi_\phi}^1$) performs the tasks
 224 comparably with **ALAC**. Nevertheless, more strict constraints (**ALAC**($\Delta\mathcal{L}_{\pi_\phi}^1$)) negatively affect
 225 its performance on constraint violations, as shown in Figure 3. This is because there doesn't exist
 226 a reasonable policy that meets such strict constraints. Moreover, the results of **ALAC**($k = 0.1$)
 227 comparing with **ALAC** demonstrate that the heuristic updating of k is effective during the training.

228 5.3 Evaluation Results

229 In this section, we describe the impacts of the stability condition more concretely by using vari-
 230 ous visualization methods. Furthermore, we verify that **ALAC** achieves excellent robustness and
 231 generalization.

232 **Analysis of Visualization:** First, we use the t-SNE method to indicate the visualization of the state in
 233 3 dimensions in order to illustrate better the stability of the system learned by **ALAC** (**Cartpole-cost**
 234 in 2 dimensions). As we can see, the top row of Figure 4 shows the states in the final stage of
 235 an episode converge to a point or circle. Basically, we recognize that those patterns happen in a
 236 stable system. The second row of Figure 4 shows the phase trajectories with variance according
 237 to the state pairs of joint angular position and velocity. In practice, experts can judge a system's
 238 stability from a phase space of the system. Concretely, ψ and $\dot{\psi}$ represent an angular position and
 239 velocity, respectively. The angular velocity starts from 0 to 0, and the angular position starts from the
 240 beginning to an equilibrium point. Based on the above phenomenons, it suggests the trained systems
 241 using the **ALAC** method satisfy focal stability or stable limit cycles. Furthermore, the Lyapunov
 242 value exhibits significant changes in the state space, as depicted in Figure 4 (bottom row). It indicates
 243 that the Lyapunov value can effectively guide the policy towards discovering stable patterns in the
 244 system. More implementation details for t-SNE and phase trajectories are given in Appendix E.5.

245 **Robustness:** Generally speaking, stability has a potential relationship with robustness to some extent
 246 [10]. Thus, we add external disturbances with different magnitudes in each environment and observe
 247 the performance difference. Figure 8 (see Appendix E.6.1) shows in all scenarios, **ALAC** enjoys
 248 superior performance over other methods.

249 **Generalization:** Furthermore, some experiments verify that the policy can generalize well to follow
 250 previously unseen reference signals. We introduce the error between the desired and achieved goals
 251 as additional information in the state. Because the Lyapunov function is significantly related to the
 252 error, **ALAC w/ errors** gains remarkable performance improvement on generalization as Table 2
 253 illustrated. We choose the **SAC-cost** algorithm as a comparison since **SAC-cost** is very similar to
 254 our method without sampling-based stability. In particular, the gap between each other enlarges with
 255 the increasing biases. Furthermore, we observe that the errors harm the performance of **SAC-cost**
 256 on complex tasks like **Halfcheetah-cost** and **Spacereach-cost**. For more experimental results, see
 257 Appendix E.6.2.

258 6 Discussion and Future Work

259 We propose a sampling-based Lyapunov stability condition to meet the mean cost stability. Based
 260 on the condition, the policy optimization with sampling-based stability is proposed to gradually
 261 find the optimal policy which maintains the *optimal-time stability* we propose. Based on the Actor-
 262 Critic framework and Lagrangian-based optimization, We present a practical algorithm, namely the
 263 Adaptive Lyapunov-based Actor-Critic algorithm (**ALAC**). Despite the great success in simulated
 264 tasks, our method is not evaluated in practical scenarios. An important direction for future work
 265 is to apply our method to some robotic control tasks like locomotion and navigation, which can
 266 demonstrate the robustness and generalization ability of the method we verified in this paper. Another
 267 future work on theoretical improvement is to combine the policy optimization with stability guarantee
 268 and safety criteria.

References

- 269
- 270 [1] J. Hwangbo, J. Lee, A. Dosovitskiy, D. Bellicoso, V. Tsounis, V. Koltun, and M. Hutter. Learning
271 agile and dynamic motor skills for legged robots. *Science Robotics*, 4(26):eaau5872, 2019.
- 272 [2] O. M. Andrychowicz, B. Baker, M. Chociej, R. Jozefowicz, B. McGrew, J. Pachocki, A. Petron,
273 M. Plappert, G. Powell, A. Ray, et al. Learning dexterous in-hand manipulation. *The International
274 Journal of Robotics Research*, 39(1):3–20, 2020.
- 275 [3] W. Jin, Z. Wang, Z. Yang, and S. Mou. Neural certificates for safe control policies. *arXiv
276 preprint arXiv:2006.08465*, 2020.
- 277 [4] J. La Salle and S. Lefschetz. *Stability by Liapunov’s Direct Method with Applications by Joseph
278 L. Salle and Solomon Lefschetz*. Elsevier, 2012.
- 279 [5] H. Dai, B. Landry, L. Yang, M. Pavone, and R. Tedrake. Lyapunov-stable neural-network
280 control. *arXiv preprint arXiv:2109.14152*, 2021.
- 281 [6] S. Lale, Y. Shi, G. Qu, K. Azizzadenesheli, A. Wierman, and A. Anandkumar. Krcrl: Krasovskii-
282 constrained reinforcement learning with guaranteed stability in nonlinear dynamical systems.
283 *arXiv preprint arXiv:2206.01704*, 2022.
- 284 [7] N. Gaby, F. Zhang, and X. Ye. Lyapunov-net: A deep neural network architecture for lyapunov
285 function approximation. *arXiv preprint arXiv:2109.13359*, 2021.
- 286 [8] R. Zhou, T. Quartz, H. De Sterck, and J. Liu. Neural lyapunov control of unknown nonlinear
287 systems with stability guarantees. *arXiv preprint arXiv:2206.01913*, 2022.
- 288 [9] M. Han, L. Zhang, J. Wang, and W. Pan. Actor-critic reinforcement learning for control with
289 stability guarantee. *IEEE Robotics and Automation Letters*, 5(4):6217–6224, 2020.
- 290 [10] Y.-C. Chang and S. Gao. Stabilizing neural control using self-learned almost lyapunov critics.
291 In *2021 IEEE International Conference on Robotics and Automation (ICRA)*, pages 1803–1809.
292 IEEE, 2021.
- 293 [11] Z. Xiong, J. Eappen, A. H. Qureshi, and S. Jagannathan. Model-free neural lyapunov control
294 for safe robot navigation. *arXiv preprint arXiv:2203.01190*, 2022.
- 295 [12] T. Zhao, J. Wang, X. Lu, and Y. Du. Neural lyapunov control for power system transient stability:
296 A deep learning-based approach. *IEEE Transactions on Power Systems*, 37(2):955–966, 2021.
- 297 [13] M. Han, Y. Tian, L. Zhang, J. Wang, and W. Pan. Reinforcement learning control of constrained
298 dynamic systems with uniformly ultimate boundedness stability guarantee. *Automatica*, 129:
299 109689, 2021.
- 300 [14] S. P. Bhat and D. S. Bernstein. Finite-time stability of continuous autonomous systems. *SIAM
301 Journal on Control and optimization*, 38(3):751–766, 2000.
- 302 [15] A. Stooke, J. Achiam, and P. Abbeel. Responsive safety in reinforcement learning by pid
303 lagrangian methods. In *International Conference on Machine Learning*, pages 9133–9143.
304 PMLR, 2020.
- 305 [16] H. Sikchi, W. Zhou, and D. Held. Lyapunov barrier policy optimization. *arXiv preprint
306 arXiv:2103.09230*, 2021.
- 307 [17] Y. Chow, O. Nachum, A. Faust, E. Duenez-Guzman, and M. Ghavamzadeh. Lyapunov-based
308 safe policy optimization for continuous control. *arXiv preprint arXiv:1901.10031*, 2019.
- 309 [18] T. Haarnoja, A. Zhou, P. Abbeel, and S. Levine. Soft actor-critic: Off-policy maximum entropy
310 deep reinforcement learning with a stochastic actor. In *International conference on machine
311 learning*, pages 1861–1870. PMLR, 2018.

- 312 [19] S. M. Richards, F. Berkenkamp, and A. Krause. The lyapunov neural network: Adaptive
313 stability certification for safe learning of dynamical systems. In *Conference on Robot Learning*,
314 pages 466–476. PMLR, 2018.
- 315 [20] Y.-C. Chang, N. Roohi, and S. Gao. Neural lyapunov control. *Advances in neural information*
316 *processing systems*, 32, 2019.
- 317 [21] M. Mittal, M. Gallieri, A. Quaglino, S. S. M. Salehian, and J. Koutník. Neural lyapunov model
318 predictive control. 2020.
- 319 [22] H. Dai, B. Landry, M. Pavone, and R. Tedrake. Counter-example guided synthesis of neural
320 network lyapunov functions for piecewise linear systems. In *2020 59th IEEE Conference on*
321 *Decision and Control (CDC)*, pages 1274–1281. IEEE, 2020.
- 322 [23] M. Lechner, Đ. Žikelić, K. Chatterjee, and T. A. Henzinger. Stability verification in stochastic
323 control systems via neural network supermartingales. *arXiv preprint arXiv:2112.09495*, 2021.
- 324 [24] P. L. Donti, M. Roderick, M. Fazlyab, and J. Z. Kolter. Enforcing robust control guarantees
325 within neural network policies. In *International Conference on Learning Representations*, 2020.
- 326 [25] K. Kashima, R. Yoshiuchi, and Y. Kawano. Learning stabilizable deep dynamics models. *arXiv*
327 *preprint arXiv:2203.09710*, 2022.
- 328 [26] S. Chen, M. Fazlyab, M. Morari, G. J. Pappas, and V. M. Preciado. Learning region of attraction
329 for nonlinear systems. In *2021 60th IEEE Conference on Decision and Control (CDC)*, pages
330 6477–6484. IEEE, 2021.
- 331 [27] N. Lawrence, P. Loewen, M. Forbes, J. Backstrom, and B. Gopaluni. Almost surely stable deep
332 dynamics. *Advances in Neural Information Processing Systems*, 33:18942–18953, 2020.
- 333 [28] A. Schlaginhaufen, P. Wenk, A. Krause, and F. Dorfler. Learning stable deep dynamics
334 models for partially observed or delayed dynamical systems. *Advances in Neural Information*
335 *Processing Systems*, 34:11870–11882, 2021.
- 336 [29] F. Berkenkamp, M. Turchetta, A. Schoellig, and A. Krause. Safe model-based reinforcement
337 learning with stability guarantees. *Advances in neural information processing systems*, 30,
338 2017.
- 339 [30] C. Dawson, Z. Qin, S. Gao, and C. Fan. Safe nonlinear control using robust neural lyapunov-
340 barrier functions. In *Conference on Robot Learning*, pages 1724–1735. PMLR, 2022.
- 341 [31] Y. Chow, O. Nachum, E. Duenez-Guzman, and M. Ghavamzadeh. A lyapunov-based approach
342 to safe reinforcement learning. *Advances in neural information processing systems*, 31, 2018.
- 343 [32] M. Han, Z. Zhou, L. Zhang, J. Wang, and W. Pan. Reinforcement learning for control with
344 probabilistic stability guarantee. 2020.
- 345 [33] T. Huang, S. Gao, X. Long, and L. Xie. A neural lyapunov approach to transient stability
346 assessment in interconnected microgrids. In *HICSS*, pages 1–10, 2021.
- 347 [34] X. Li, J. Xiao, Y. Cheng, and H. Liu. An actor-critic learning framework based on lyapunov
348 stability for automatic assembly. *Applied Intelligence*, pages 1–12, 2022.
- 349 [35] L. Zhang, R. Zhang, T. Wu, R. Weng, M. Han, and Y. Zhao. Safe reinforcement learning with
350 stability guarantee for motion planning of autonomous vehicles. *IEEE Transactions on Neural*
351 *Networks and Learning Systems*, 32(12):5435–5444, 2021.
- 352 [36] R. M. Murray, Z. Li, and S. S. Sastry. *A mathematical introduction to robotic manipulation*.
353 CRC press, 2017.

- 354 [37] S. Zou, T. Xu, and Y. Liang. Finite-sample analysis for sarsa with linear function approximation.
355 *Advances in neural information processing systems*, 32, 2019.
- 356 [38] S. Wang, Y. Cao, X. Zheng, and T. Zhang. Collision-free trajectory planning for a 6-dof free-
357 floating space robot via hierarchical decoupling optimization. *IEEE Robotics and Automation*
358 *Letters*, 7(2):4953–4960, 2022.
- 359 [39] G. Brockman, V. Cheung, L. Pettersson, J. Schneider, J. Schulman, J. Tang, and W. Zaremba.
360 Openai gym. *arXiv preprint arXiv:1606.01540*, 2016.
- 361 [40] J. Achiam, D. Held, A. Tamar, and P. Abbeel. Constrained policy optimization. In *International*
362 *conference on machine learning*, pages 22–31. PMLR, 2017.
- 363 [41] E. Coumans and Y. Bai. Pybullet, a python module for physics simulation for games, robotics
364 and machine learning. 2016.
- 365 [42] J. Schulman, S. Levine, P. Abbeel, M. Jordan, and P. Moritz. Trust region policy optimization.
366 In *International conference on machine learning*, pages 1889–1897. PMLR, 2015.
- 367 [43] J. Schulman, F. Wolski, P. Dhariwal, A. Radford, and O. Klimov. Proximal policy optimization
368 algorithms. *arXiv preprint arXiv:1707.06347*, 2017.

369 **A Related Work**

370 Learning-based controllers have achieved excellent performance in non-linear dynamic systems [1, 2].
371 However, a lack of stability introduces additional risks to the agents and environments [3]. Fortunately,
372 there exists an effective tool, Lyapunov functions, to assess the stability. Lyapunov functions can be
373 designed for a linear system with specific criteria in the form of a quadratic positive-definite function.
374 But how to find a suitable Lyapunov function remains an open challenge in the non-linear dynamic
375 system [4].

376 **A.1 Model-based RL & Lyapunov Learning**

377 Due to the difficulty of a manual design, constructing a Lyapunov neural network has become
378 increasingly popular in a non-linear dynamic system. For the model-known situation, the approaches
379 jointly learn a Lyapunov function and a controller [19, 20, 21, 22, 23, 24, 7]. But it restricts the
380 application of complex systems which are hard to obtain accurate models. Therefore, some researchers
381 present model-learned methods with a stability guarantee, in which Gaussian Process or Neural
382 Network approximates the model. The model-learned method can be separated into two types. The
383 first one is learning dynamics models guided by a learnable Lyapunov function, in which policies are
384 inherently included or learned by LQR method [25, 8, 26, 27, 28]. Another approach is to construct a
385 learnable policy network updated by a neural Lyapunov function, thereby satisfying the stability of
386 system [29, 30, 8, 5, 6]. However, we notice that most model-learned methods are only verified in
387 relatively easy environments. A possible reason is that the coupling of the Lyapunov function and
388 dynamic model makes learning unstable or incompatible due to interdependency.

389 **A.2 Model-free RL & Lyapunov Learning**

390 A promising direction is to study model-free methods with a stability guarantee. Recently, a large
391 variety of methods have been proposed to address the issue. One method is that the policy is updated
392 by a mixed objective with respect to the neural Lyapunov function and Q function. POLYC [10]
393 introduced the necessary conditions required by the Lyapunov function into objectives to optimize
394 the policy network. LBPO [16] applied the logarithmic barrier function based on the form of the
395 Lyapunov function. TNLf [11] constructed Lyapunov V and Q functions trained by the stability
396 certification. The other form is policy optimization with Lyapunov constraints. Chow et al. [31]
397 designed a constrained RL algorithm to project a policy in a trust region with Lyapunov stability.
398 In those previous study, there still exist a main drawback. The discrete Lyapunov condition they
399 used did not meet the demand for a sampling-based stability guarantee in RL. Therefore, Han et al.
400 [9] considered a sampling-based stability condition they proposed as a constraint and then used the
401 prime-dual method to modify the constraint. Their latter work verified them in both on-policy and
402 off-policy settings [13, 32]. Nevertheless, their method can only find an existing policy with the
403 demand for stability. In contrast, our method can satisfy the sampling-based stability and search for
404 the optimal policy adaptively. The optimal policy can facilitate the state to reach the equilibrium
405 point rapidly.

406 **A.3 Applications**

407 Furthermore, it is worth noting that current RL-based methods with stability guarantee have been
408 applied in some practical problems successfully, such as monitoring the security of interconnected
409 microgrids [33], power system control [12], automatic assembly [34] and motion planning of au-
410 tonomous vehicles [35].

411 B Preliminary Remarks

412 B.1 Lyapunov function

413 **Definition B.1** (Equilibrium Point). A state s_e is an equilibrium point if \exists action $a_e \in \mathcal{A}$ such that
 414 $f(s_e, a_e) = s_e$. [36]

415 **Definition B.2** (Stabilizable in the sense of Lyapunov). A system is stabilizable if $\forall \epsilon > 0, \exists \delta$ such
 416 that for all $s_0 \in \mathcal{S}$ such that $\|s_0 - s_e\| \leq \delta$, there exists $\{a_t\}_{t=0}^{\infty}$ such that the resulting $\{s_t\}_{t=0}^{\infty}$
 417 satisfies $\|s_t - s_e\| \leq \epsilon \forall t \geq 0$. [36]

418 **Definition B.3** (Lyapunov Function). A continuous and radially unbounded function $\mathcal{L} : \mathcal{S} \rightarrow \mathbb{R}$ is a
 419 Lyapunov function if the following conditions hold:

- 420 1. $\forall s \in \mathcal{S}, \exists a \in \mathcal{A}$, s.t. $\mathcal{L}(s) \geq \mathcal{L}(f(s, a))$,
- 421 2. $\forall s \neq 0, \mathcal{L} > 0; \mathcal{L}(0) = 0$.

422 If a Lyapunov function exists, a discrete-time system can achieve stability in the sense of Lyapunov
 423 without considering the physical energy.

424 B.2 Lyapunov Candidate Bound

425 In this part, we show that the Lyapunov candidate $\mathcal{L}_\pi(s)$ meets the property in Theorem 3.1, which
 426 can be formulated as:

$$c_\pi(s) + \lambda \mathbb{E}_{s' \sim \mathcal{P}_\pi} \mathcal{L}(s') \leq \mathcal{L}(s) \leq \beta c_\pi(s) \quad (15)$$

427 where we omit the lower bound $\alpha c_\pi(s)$ which is naturally satisfied by $\mathcal{L}_\pi(s)$.

428 Firstly, according to the definition of $\mathcal{L}_\pi(s)$, we have

$$\begin{aligned} \mathcal{L}_\pi(s) &= \mathbb{E}_\pi \left[\sum_{t=0}^{\infty} \gamma^t c_\pi(s_t) \mid s_0 = s \right] \\ &= \mathbb{E}_\pi \left[c_\pi(s_0) + \sum_{t=1}^{\infty} \gamma^t c_\pi(s_t) \mid s_0 = s \right] \\ &= c_\pi(s) + \mathbb{E}_\pi \left[\sum_{t=1}^{\infty} \gamma^t c_\pi(s_t) \right] \\ &= c_\pi(s) + \gamma \mathbb{E}_{\pi, s' \sim \mathcal{P}_\pi} \left[\sum_{t=0}^{\infty} \gamma^t c_\pi(s_t) \mid s_0 = s' \right] \\ &= c_\pi(s) + \gamma \mathbb{E}_{s' \sim \mathcal{P}_\pi} \mathcal{L}(s') \end{aligned} \quad (16)$$

429 Considering the left-hand side of Equation (4), we can find that if $\lambda \leq \gamma$ holds, the lower bound of the
 430 Lyapunov function can be satisfied. This is because the Lyapunov candidate $\mathcal{L}_\pi(s)$ is positive at each
 431 state. Furthermore, the right-hand side of Equation 4 illustrates the higher bound of the Lyapunov
 432 function exists. The condition is also guaranteed for our Lyapunov candidate shown in the following
 433 process.

$$\begin{aligned} \mathcal{L}_\pi(s) &= \mathbb{E}_\pi \left[\sum_{t=0}^{\infty} \gamma^t c_\pi(s_t) \mid s_0 = s \right] \\ &\leq \sum_{t=0}^{\infty} \gamma^t \mathbb{E}_\pi [c_\pi(s_t) \mid s_0 = s] \\ &\leq \frac{\bar{c}_\pi}{1 - \gamma} \end{aligned} \quad (17)$$

434 Note that \bar{c}_π denotes the maximum cost. The second row of the inequality holds due to Jensen
 435 inequality. Only if the maximum cost exists, $\exists \beta \in \mathbb{R}_+, \frac{\bar{c}_\pi}{1 - \gamma} \leq \beta c_\pi(s)$ holds.

436 C Details of Theoretical Analysis

437 C.1 Assumptions of Theorem 3.1

438

439 **Assumption C.1** (Region of Attraction). There exists a positive constant b such that $\rho(s) > 0, \forall s \in$
 440 $\{s | c_\pi(s) \leq b\}$.

441 **Assumption C.2** (Ergodic Property). The Markov Chain driven by the policy π is ergodic, $\omega_\pi(s) =$
 442 $\lim_{t \rightarrow \infty} \mathcal{T}(s | \rho, \pi, t)$.

443 The first one ensures that the starting state is sampled in the region of attraction. The second one is
 444 the existence of the stationary state distribution.

445 C.2 Proof of Theorem 3.1

446 **Theorem C.3** (Sampling-based Lyapunov Stability). *An MDP system is stable with regard to the*
 447 *mean cost, if there exists a function $\mathcal{L} : S \rightarrow \mathbb{R}$ meets the following conditions:*

$$448 \quad \alpha c_\pi(s) \leq \mathcal{L}(s) \leq \beta c_\pi(s) \quad (18)$$

$$449 \quad \mathcal{L}(s) \geq c_\pi(s) + \lambda \mathbb{E}_{s' \sim \mathcal{P}_\pi} \mathcal{L}(s') \quad (19)$$

$$449 \quad \mathbb{E}_{s \sim \mathcal{U}_\pi} [\mathbb{E}_{s' \sim \mathcal{P}_\pi} \mathcal{L}(s') - \mathcal{L}(s)] \leq -k [\mathbb{E}_{s \sim \mathcal{U}_\pi} [\mathcal{L}(s) - \lambda \mathbb{E}_{s' \sim \mathcal{P}_\pi} \mathcal{L}(s')]] \quad (20)$$

450 where α, β, λ and k is positive constants. Among them, $\mathcal{P}_\pi(s'|s) = \int_{\mathcal{A}} \pi(a|s) \mathcal{P}(s'|s, a) da$ holds.

451 *Proof.* Firstly, we simplify the left side of the Equation (20) with reference to [9]. Introducing the
 452 definition of $\mathcal{U}_\pi(s)$ leads to

$$\begin{aligned} & \mathbb{E}_{s \sim \mathcal{U}_\pi} [\mathbb{E}_{s' \sim \mathcal{P}_\pi} \mathcal{L}_\pi(s') - \mathcal{L}_\pi(s)] \\ &= \int_S \lim_{T \rightarrow \infty} \frac{1}{T} \sum_{t=0}^T \mathcal{T}(s | \rho, \pi, t) \left(\int_S \mathcal{P}_\pi(s'|s) \mathcal{L}_\pi(s') ds' - \mathcal{L}_\pi(s) \right) ds \end{aligned} \quad (21)$$

453 Due to the boundedness of \mathcal{L}_π , we apply the Lebesgue's Dominated convergence theorem. To be
 454 specific, when $|F_n(s)| \leq B(s), \forall s \in S, \forall n$ holds, we have

$$\lim_{n \rightarrow \infty} \int_S F_n(s) ds = \int_S \lim_{n \rightarrow \infty} F_n(s) ds \quad (22)$$

455 Hence, we get

$$\begin{aligned} & \mathbb{E}_{s \sim \mathcal{U}_\pi} [\mathbb{E}_{s' \sim \mathcal{P}_\pi} \mathcal{L}_\pi(s') - \mathcal{L}_\pi(s)] \\ &= \int_S \lim_{T \rightarrow \infty} \frac{1}{T} \sum_{t=0}^T \mathcal{T}(s | \rho, \pi, t) \left(\int_S \mathcal{P}_\pi(s'|s) \mathcal{L}_\pi(s') ds' - \mathcal{L}_\pi(s) \right) ds \\ &= \lim_{T \rightarrow \infty} \int_S \frac{1}{T} \sum_{t=0}^T \mathcal{T}(s | \rho, \pi, t) \left(\int_S \mathcal{P}_\pi(s'|s) \mathcal{L}_\pi(s') ds' - \mathcal{L}_\pi(s) \right) ds \\ &= \lim_{T \rightarrow \infty} \frac{1}{T} \left(\sum_{t=1}^{T+1} \mathbb{E}_{\mathcal{T}(s|\rho, \pi, t)} \mathcal{L}_\pi(s) - \sum_{t=0}^T \mathbb{E}_{\mathcal{T}(s|\rho, \pi, t)} \mathcal{L}_\pi(s) \right) \\ &= \lim_{T \rightarrow \infty} \frac{1}{T} \left(\mathbb{E}_{\mathcal{T}(s|\rho, \pi, T+1)} \mathcal{L}_\pi(s) - \mathbb{E}_{\mathcal{T}(s|\rho, \pi, t=0)} \mathcal{L}_\pi(s) \right) \end{aligned} \quad (23)$$

456 Note that $\mathcal{T}(s|\rho, \pi, t=0)$ is equal to ρ . Since the expectation of $\mathcal{L}_\pi(s)$ is a finite value, the left side
 457 of Equation (20) is zero.

458 Now, we turn to the right side of Equation (20). According to the Equation (23), we have

$$\begin{aligned} -k[\mathbb{E}_{s \sim \mathcal{U}_\pi}[\mathcal{L}(s) - \lambda \mathbb{E}_{s' \sim \mathcal{P}_\pi} \mathcal{L}(s')]] &\geq 0 \\ \mathbb{E}_{s \sim \mathcal{U}_\pi}[\mathcal{L}(s) - \lambda \mathbb{E}_{s' \sim \mathcal{P}_\pi} \mathcal{L}(s')] &\leq 0 \end{aligned} \quad (24)$$

459 Since $\mathcal{L}(s) \geq c_\pi(s) + \lambda \mathbb{E}_{s' \sim \mathcal{P}_\pi} \mathcal{L}(s')$ holds, we get

$$\mathbb{E}_{s \sim \mathcal{U}_\pi} c_\pi(s) \leq 0 \quad (25)$$

460 Based on the Abelian theorem, we know there exists

$$\begin{aligned} \mathcal{U}_\pi(s) &= \lim_{T \rightarrow \infty} \frac{1}{T} \sum_{t=0}^T \mathcal{T}(s | \rho, \pi, t) \\ &= \lim_{t \rightarrow \infty} \mathcal{T}(s | \rho, \pi, t) \\ &= \omega_\pi(s) \end{aligned} \quad (26)$$

461 Thus, we get

$$\mathbb{E}_{s \sim \omega_\pi} [c_\pi(s)] \leq 0 \quad (27)$$

462 The last row of inequality holds because of Equation (26). Based on the definition of $\omega_\pi(s)$, we have

$$\lim_{t \rightarrow \infty} \mathbb{E}_{\mathcal{T}(s|\rho,\pi,t)} c_\pi(s) \leq 0 \quad (28)$$

463 Suppose that there exists a starting state $s_0 \in \{s_0 \mid c_\pi(s_0) \leq b\}$ and a positive constant d such that
464 $\lim_{t \rightarrow \infty} \mathbb{E}_{\mathcal{T}(s|\rho,\pi,t)} c_\pi(s) = d$ or $\lim_{t \rightarrow \infty} \mathbb{E}_{\mathcal{T}(s|\rho,\pi,t)} c_\pi(s) = \infty$. Consider that $\rho(s_0) > 0$ for all
465 starting states in $\{s_0 \mid c_\pi(s_0) \leq b\}$ (Assumption C.1), then $\lim_{t \rightarrow \infty} \mathbb{E}_{s \sim \mathcal{T}(\cdot|\rho,\pi,t)} c_\pi(s) > 0$, which
466 is contradictory with Equation (28). Thus $\forall s_0 \in \{s_0 \mid c_\pi(s_0) \leq b\}$, $\lim_{t \rightarrow \infty} \mathbb{E}_{\mathcal{T}(s|\rho,\pi,t)} c_\pi(s) = 0$.
467 Thus the system meets the mean cost stability by Definition 2.1.

468 Furthermore, we find that when $\mathcal{L}(s) = c_\pi(s) + \lambda \mathbb{E}_{s' \sim \mathcal{P}_\pi} \mathcal{L}(s')$ holds, our theorem is corresponding
469 to the Theorem 1 in [9]. That means we extend the previous method to a more general case. To be
470 specific, the introduction of λ enlarges the solution space of the policy. Thus, it facilitates the policy
471 to find the optimal point as well as maintain the system's stability.

472 □

473 C.3 Finite-Time Feedback Tracking Method

474 **Lemma C.4** (Finite-Time Feedback Tracking Method). *In a continuous-time system, a trajectory*
475 *$W(t)$ tracks the reference $R(t)$. $W(t)$ can track the reference within a finite time T , such that*
476 *$R(t) = W(t), t \geq T$, if the following conditions holds.*

$$\nabla_t W(t) \leq -k(W(t) - R(t)), \forall t \in [0, T] \quad (29)$$

477 Note that the gradient of $R(t)$ is bounded, meaning that $\nabla_t R(t) \leq \mu$ holds.

478 *Proof.* First, we build the mean square error $V(t)$ between them.

$$V = \frac{1}{2}(W(t) - R(t))^2 \quad (30)$$

479 Then, we can derive the difference of $V(t)$ as follows

$$\begin{aligned} \nabla_t V &= (W - R)(\nabla_t W - \nabla_t R) \\ &\leq (W - R)(-k(W - R) - \nabla_t R) \\ &\leq -k|W - R|^2 - (W - R)\nabla_t R \end{aligned} \quad (31)$$

480 Introducing the Assumption that the bounded gradient of $R(t)$, we have

$$\begin{aligned} \nabla_t V &\leq -2k \frac{|W - R|^2}{2} - \sqrt{2}\mu \frac{|W - R|}{2} \\ &\leq -2kV - \sqrt{2}\mu\sqrt{V} \end{aligned} \quad (32)$$

481 Observe that the above formulation belongs to a form of the Bernoulli differential equation. In this
482 case, we can reduce the Bernoulli equation to a linear differential equation by substituting $z = \sqrt{V}$.
483 Then, the general solution for z is

$$z = \sqrt{V} \leq -\frac{\sqrt{2}\mu}{2k} + Ce^{-kt} \quad (33)$$

484 Applying the initial condition $V(t = 0) = v_{t_0}$, we have

$$C = \sqrt{v_{t_0}} + \frac{\sqrt{2}\mu}{2k} \quad (34)$$

485 Finally, the convergence time T can be represented as:

$$T = \frac{1}{k} \ln \left(\frac{\frac{\sqrt{2}\mu}{2k} + \sqrt{v_{t_0}}}{\frac{\sqrt{2}\mu}{2k}} \right) + t_0 \quad (35)$$

486

□

487 C.4 Illustration of the Feedback Tracking

488 First, we denote $W(t)$ as $\mathcal{L}_\pi(s)$, $W(t + 1)$ as $\mathcal{L}_\pi(s')$ and $R(t)$ as $\lambda\mathcal{L}_\pi(s')$, where we omit the
489 expectation operator for simplicity. Specifically, at time $t + 1$, the value of $W(t + 1)$ should decrease
490 by $k(W(t) - R(t))$. The change of λ and k results in $k(W(t) - R(t))$ increases correspondingly.
491 Consequently, $W(t + 1)$ needs to decrease further to meet the requirement. Recalling the definition,
492 $\mathcal{L}_\pi(s')$ become smaller. Additionally, the form of Equation (9) is similar to finite-time tracking
493 method in continuous-time system which we depict in Appendix C.3.

494 C.5 Constrained Lyapunov Critic Network

495 Concretely, we denote the output of a neural network as $\mathbf{f}(s, a)$. And then, $\mathcal{L}_\theta(s, a)$ can be described
496 by:

$$\mathcal{L}_\theta(s, a) = (\mathbf{G}_s(\mathbf{f}(s, a)))(\mathbf{G}_s(\mathbf{f}(s, a)))^\top \quad (36)$$

497 where \mathbf{G}_s is a linear transformation, which guarantees $\mathbf{G}_{s=s_e}(\mathbf{f}(s = s_e, a)) = \mathbf{0}$ (s_e is an equilibrium
498 point defined in Definition B.1.). Note that \mathbf{G}_s contains no parameters to be learned, so the operator
499 does not cause harm to the representation ability of the neural network.

500 Concretely, the output of the neural network of the Lyapunov critic is described by:

$$\mathbf{f}(s, a) = \mathbf{h}_O(\mathbf{h}_{O-1}(\cdots \mathbf{h}_2(\mathbf{h}_1(\langle s, a \rangle)))) \quad (37)$$

501 where each $h_o(z)$ has the same form:

$$\mathbf{h}_o(z) = \psi_o(\mathbf{W}_o z + \mathbf{b}_o) \quad (38)$$

502 Here, O represents the number of layers, and ψ_o is the non-linear activation function used in the o -th
503 layer. Furthermore, $\{\mathbf{W}_o, \mathbf{b}_o\}$ is the weight and bias of the o -th layer.

504 First of all, to meet the demand of $\mathcal{L}_\theta(s_e, a) = 0$, we introduce a linear transformation \mathbf{G}_s , one of
505 whose possible forms can be

$$\mathbf{G}_s(\mathbf{f}) = \frac{1}{\sum_i \delta s_i + \epsilon} \begin{bmatrix} \delta s_1 & \delta s_2 & \cdots & \delta s_I \end{bmatrix} \begin{bmatrix} \mathbf{f}_1 & \mathbf{f}_1 & \cdots & \mathbf{f}_v \\ \mathbf{f}_1 & \mathbf{f}_1 & \cdots & \mathbf{f}_v \\ \cdots & \cdots & \cdots & \cdots \\ \mathbf{f}_1 & \mathbf{f}_1 & \cdots & \mathbf{f}_v \end{bmatrix} \quad (39)$$

506 where I denotes the number of elements of the state, and v is the number of units of the output layer.
 507 ϵ is a constant close to 0 to avoid singularity. Note that $\delta s = s - s_e$, which indicates the difference
 508 between the current state and an equilibrium point. As we can see, when each element of δs is zero,
 509 the multiplication of matrices is zero. Thus, $\mathbf{G}_{s=s_e}(\mathbf{f}(s = s_e, a)) = \mathbf{0}$ holds. Furthermore, it brings
 510 another benefit having no impact on the training of networks.

511 C.6 Proof of Theorem 4.1

512 **Theorem C.5.** *Suppose that the length of sampling trajectories is T , then the bound can be expressed*
 513 *as:*

$$|\mathbb{E}_{s \sim \mathcal{U}_\pi} \Delta \mathcal{L}_\pi(s) - \mathbb{E}_{s \sim \mathcal{U}_\pi^T} \Delta \mathcal{L}_\pi(s)| \leq 2 \frac{(k+1)\bar{c}_\pi}{1-\gamma} T^{q-1} \quad (40)$$

514 where q is a constant in $(0, 1)$.

515 *Proof.* First, we can get the following equation by introducing the definitions of \mathcal{U}_π and \mathcal{U}_π^T .

$$\begin{aligned} & \mathbb{E}_{s \sim \mathcal{U}_\pi} \Delta \mathcal{L}_\pi(s) - \mathbb{E}_{s \sim \mathcal{U}_\pi^T} \Delta \mathcal{L}_\pi(s) \\ &= \int_{\mathcal{S}} (\mathcal{U}_\pi(s) - \frac{1}{T} \sum_{t=1}^T \mathcal{T}(s | \rho, \pi, t)) \Delta \mathcal{L}_\pi(s) ds \\ &= \frac{1}{T} \sum_{t=1}^T \int_{\mathcal{S}} (\mathcal{U}_\pi(s) - \mathcal{T}(s | \rho, \pi, t)) \Delta \mathcal{L}_\pi(s) ds \end{aligned} \quad (41)$$

516 Then, eliminating the integral operator, we obtain

$$\begin{aligned} & |\mathbb{E}_{s \sim \mathcal{U}_\pi} \Delta \mathcal{L}_\pi(s) - \mathbb{E}_{s \sim \mathcal{U}_\pi^T} \Delta \mathcal{L}_\pi(s)| \\ & \leq \frac{1}{T} \sum_{t=1}^T \|\mathcal{U}_\pi(s) - \mathcal{T}(s | \rho, \pi, t)\|_1 \|\Delta \mathcal{L}_\pi(s)\|_\infty \end{aligned} \quad (42)$$

517 Thus, the next step is to get the bounds of $\|\mathcal{U}_\pi(s) - \mathcal{T}(s | \rho, \pi, t)\|_1$ and $\|\Delta \mathcal{L}_\pi(s)\|_\infty$.

518 For the first part, we introduce the assumption that first is mentioned in [37], shown as follows:

$$\sum_{t=1}^T \|\mathcal{U}_\pi(s) - \mathcal{T}(s | \rho, \pi, t)\|_1 \leq 2T^q, \quad \forall T \in \mathcal{Z}_+, \quad \exists q \in (0, 1) \quad (43)$$

519 Frankly speaking, the assumption is easily satisfied because the L1 distance between two distributions
 520 is bounded by 2. At the same time, $\mathcal{T}(s | \rho, \pi, t)$ converges to $\mathcal{U}_\pi(s)$ with time approaching.

521 For the second part, we can get the bound of $\Delta \mathcal{L}_\pi(s)$ according to Equation 17.

$$\begin{aligned} \Delta \mathcal{L}_\pi(s) &= \mathbb{E}_{s' \sim \mathcal{P}_\pi} \mathcal{L}_\pi(s') - \mathcal{L}_\pi(s) + k(\mathcal{L}_\pi(s) - \lambda \mathbb{E}_{s' \sim \mathcal{P}_\pi}(s')) \\ &\leq \frac{\bar{c}_\pi}{1-\gamma} - 0 + k\left(\frac{\bar{c}_\pi}{1-\gamma} - 0\right) \end{aligned} \quad (44)$$

522 Then, we have

$$\|\Delta \mathcal{L}_\pi(s)\|_\infty \leq (k+1) \frac{\bar{c}_\pi}{1-\gamma} \quad (45)$$

523 Adding results in Equation 46, we finally get

$$|\mathbb{E}_{s \sim \mathcal{U}_\pi} \Delta \mathcal{L}_\pi(s) - \mathbb{E}_{s \sim \mathcal{U}_\pi^T} \Delta \mathcal{L}_\pi(s)| \leq 2 \frac{(k+1)\bar{c}_\pi}{1-\gamma} T^{q-1} \quad (46)$$

524

□

525 **C.7 Proof of Theorem 4.2**

526 **Theorem C.6.** *Suppose that the length of sampling trajectories is T and the number of trajectories*
 527 *is M , then there exists the following upper bound:*

$$\begin{aligned} & \mathbb{P}\left(\left|\frac{1}{MT} \sum_{m=1}^M \sum_{t=1}^T \Delta \mathcal{L}_\pi(s_t^m) - \mathbb{E}_{s \sim \mathcal{U}_\pi^T} \Delta \mathcal{L}_\pi(s)\right| \geq \alpha\right) \\ & \leq 2 \exp\left(-\frac{M\alpha^2(1-\gamma)^2}{((1-k\lambda)^2 + (k-1)^2)\bar{c}_\pi^2}\right) \end{aligned} \quad (47)$$

528 where s_t^m represents the state in the m -th trajectory at the timestep t .

529 *Proof.* First, eliminating $\Delta \mathcal{L}_\pi(s)$ by Equation 9, we rewrites the left side of Equation 47 as

$$\begin{aligned} \delta &= \mathbb{P}\left(\left|\frac{1}{MT} \sum_{m=1}^M \sum_{t=1}^T \Delta \mathcal{L}_\pi(s_t^m) - \mathbb{E}_{s \sim \mathcal{U}_\pi^T} \Delta \mathcal{L}_\pi(s)\right| \geq \alpha\right) \\ &= \mathbb{P}\left(\left|\frac{1}{MT} \sum_{m=1}^M \sum_{t=1}^T (\mathcal{L}_\pi(s_{t+1}) - \mathcal{L}_\pi(s_t) + k_l(\mathcal{L}_\pi(s_t) - \lambda \mathcal{L}_\pi(s_{t+1}))) - \mathbb{E}_{s \sim \mathcal{U}_\pi^T} \Delta \mathcal{L}_\pi(s)\right| \geq \alpha\right) \\ &= \mathbb{P}\left(\left|\frac{1}{MT} \sum_{m=1}^M \sum_{t=1}^T ((1-k\lambda)\mathcal{L}_\pi(s_{t+1}) + (k-1)\mathcal{L}_\pi(s_t)) - \mathbb{E}_{s \sim \mathcal{U}_\pi^T} \Delta \mathcal{L}_\pi(s)\right| \geq \alpha\right) \end{aligned} \quad (48)$$

530 Here $\mathbb{E}_{s \sim \mathcal{U}_\pi^T} \Delta \mathcal{L}_\pi(s)$ is expected value of $\frac{1}{MT} \sum_{m=1}^M \sum_{t=1}^T \Delta \mathcal{L}_\pi(s_t^m)$. In addition, the bounds of
 531 $(1-k\lambda)\mathcal{L}_\pi(s_{t+1})$ and $(k-1)\mathcal{L}_\pi(s_t)$ can be obtained easily by Equation 17. Thus, we obtain the
 532 Theorem 4.2 by applying Hoeffding's inequality.

$$\begin{aligned} \delta &\leq 2 \exp\left(-\frac{2M^2\alpha^2}{M((1-k\lambda)^2 + (k-1)^2)\frac{\bar{c}_\pi^2}{(1-\gamma)^2}}\right) \\ &\leq 2 \exp\left(-\frac{M\alpha^2(1-\gamma)^2}{((1-k\lambda)^2 + (k-1)^2)\bar{c}_\pi^2}\right) \end{aligned} \quad (49)$$

533

□

534 **D Details of Algorithms**

535 As mentioned in the main text, we introduce a minimum entropy as a constraint in policy optimization
 536 and apply the primal-dual method to update the policy and the Lagrange multiplier λ_e . To be specific,
 537 the constraint can be expressed as

$$\log \pi_\phi(a|s) \leq -\mathcal{Z}_e \quad (50)$$

538 where \mathcal{Z}_e is the minimum value of policy entropy, usually, \mathcal{Z}_e corresponds to the dimension of action
 539 space in the environment.

Algorithm 1: Adaptive Lyapunov-based Actor-Critic Algorithm (ALAC)

Orthogonal initialize the parameters of actor and critic networks with ϕ, θ
Initialize replay buffer D and $\lambda_l, \lambda_e, \lambda$ and k
Initialize the parameters of target network with $\phi' \leftarrow \phi$ and $\theta' \leftarrow \theta$
for episode $m = 1, M$ **do**
 Sample an initial state s_0
 for step $t = 0, T - 1$ **do**
 Sample an action from $\pi_\phi(a_t|s_t)$
 Execute the action a_t and observe a new state s_{t+1}
 Store $\langle s_t, a_t, c_t, s_{t+1} \rangle$ into \mathcal{D}
 end for
 for iteration $n = 1, N$ **do**
 Sample a minibatch \mathcal{B} from the replay buffer D
 Update θ according to Eq.(10) using minibatch \mathcal{B}
 Update $\phi, \lambda_l, \lambda_e$ according to Eq.(11),(12),(50) using minibatch \mathcal{B}
 Update adaptive factors λ and k
 Update the parameters of target networks, θ', ϕ' .
 end for
end for

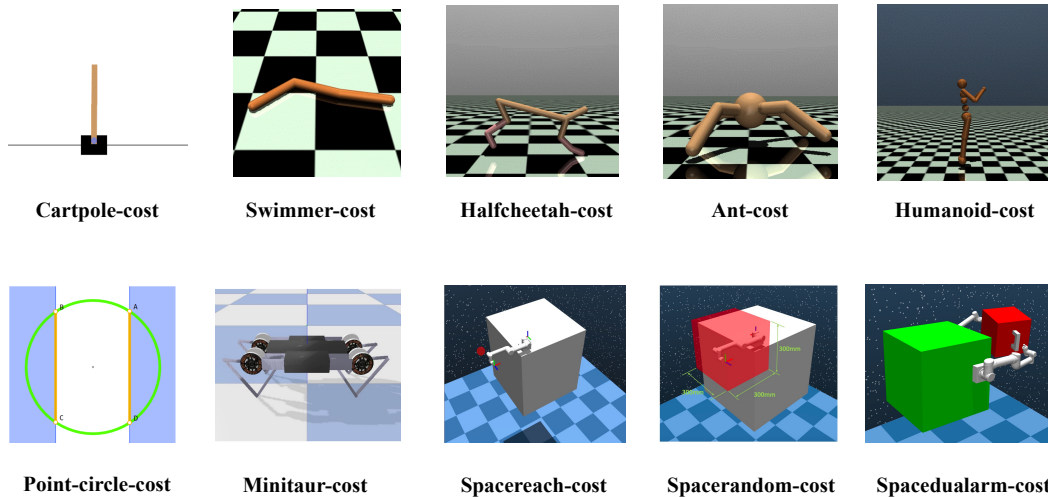
541 **E Details of Experiments**

Figure 5: Overview of our environments.

542 We test our method and baselines in ten robotic control environments, including **Cartpole-**
543 **cost**, **Point-circle-cost**, **Halfcheetah-cost**, **Swimmer-cost**, **Ant-cost**, **Humanoid-cost**, **Minitaur-cost**,
544 **Spacereach-cost**, **Spacerandom-cost** and **Spacedualarm-cost**. Most tasks in ten environments are
545 goal-oriented, tracking a target position or speed, which corresponds to most control tasks. Further-
546 more, the latter four environments involve models of practical robots like a quadruped robot and a
547 robotic arm, making them relatively more difficult. It is worth noting that the task of **Spacedualarm-**
548 **cost** is trajectory planning of a free-floating dual-arm space robot. The coupling property of the base
549 and the robotic arms brings hardship for both traditional control and RL-based methods [38].

550 **E.1 Environmental Design**

551 **Cartpole-cost** This task aims to maintain the pole vertically at a target position. The environment
552 is inherited from [32]. The state and action space are the same as the default settings in OpenAI

553 Gym[39], so we omit the description. The cost function is $c = \left(\frac{x}{x_{\text{threshold}}}\right)^2 + 20 * \left(\frac{\theta}{\theta_{\text{threshold}}}\right)^2$, where
 554 $x_{\text{threshold}} = 10$ and $\theta_{\text{threshold}} = 20^\circ$. The other settings can be found in Table 3.

555 **Point-circle-cost** This task aims to allow a sphere to track a circular trajectory. The environment is
 556 inherited from [40]. The sphere is initialized at the original point. The cost function is represented
 557 as $c = d$, where d denotes the distance between the current position and the reference. The other
 558 settings can be found in Table 3.

Table 3: Hyper-parameters of non-linear dynamic environments

Hyper-parameters	Cartpole-cost	Point-circle-cost
State shape	4	7
Action shape	2	2
Length of an episode	250 steps	65 steps
Maximum steps	3e5 steps	3e5 steps
Actor network	(64, 64)	(64, 64)
Critic network	(64, 64, 16)	(64, 64, 16)

559 **Halfcheetah-cost** The goal of this task is to make a HalfCheetah (a 2-legged simulated robot) to
 560 track the desired velocity. The environment is inherited from [32]. The state and action space are the
 561 same as the default settings in OpenAI Gym[39], so we omit the description. The cost function is
 562 $c = (v - 1)^2$, where 1 represents the desired velocity. The other settings can be found in Table 4.

563 **Swimmer-cost** This task aims to make a multi-joint snake robot to track the desired velocity. The
 564 environment is inherited from [32]. The state and action space are the same as the default settings in
 565 OpenAI Gym[39], so we omit the description. The cost function is $c = (v - 1)^2$, where 1 represents
 566 the desired velocity. The other settings can be found in Table 4.

567 **Ant-cost** This task aims to make an Ant (a quadrupedal simulated robot) track the desired velocity.
 568 The environment is inherited from [39]. The state and action space are the same as the default
 569 settings in OpenAI Gym [39], so we omit the description. The cost function is $c = (v - 1)^2$, where 1
 570 represents the desired velocity. The other settings can be found in Table 4.

571 **Humanoid-cost** This task aims to make a humanoid robot to track the desired velocity. The
 572 environment is inherited from [39]. The state and action space are the same as the default settings in
 573 OpenAI Gym [39], so we omit the description. The cost function is $c = (v - 1)^2$, where 1 represents
 574 the desired velocity. The other settings can be found in Table 4.

575 **Minitaur-cost** This task aims to control the Ghost Robotics Minitaur quadruped to run forward at
 576 the desired velocity. The environment is inherited from [41]. The state and action space are the same
 577 as the default settings in PyBullet environment[41], so we omit the description. The cost function is
 578 $c = (v - 1)^2$, where 1 represents the desired velocity. The other settings can be found in Table 5.

579 **Spacereach-cost** This task aims to make a free-floating single-arm space robot’s end-effector reach
 580 a fixed goal position. Since the base satellite is uncontrolled, collisions will cause system instability
 581 once collisions occur. Therefore, it is critical to plan a collision-free path while maintaining the
 582 stability of the base. The agent can obtain the state, including the angular positions and velocities of
 583 joints, the position of the end-effector, and the position of the reference point. Then, the agent outputs
 584 the desired velocities of joints. In low-level planning, a PD controller converts the desired velocities
 585 into torques, and then controls the manipulator. The cost function is defined as $c = d$, where d is the
 586 distance between the goal and end-effector. The other settings can be found in Table 5.

587 **Spacerandom-cost** This task aims to make a free-floating single-arm space robot’s end-effector
 588 reach a random goal position. The agent can obtain the state, including the angular positions and

Table 4: Hyper-parameters of mujoco environments

Hyper-parameters	Swimmer-cost	Halfcheetah-cost	Ant-cost	Humanoid-cost
State shape	8	17	27	376
Action shape	2	6	8	8
Length of an episode	250 steps	200 steps	200 steps	500 steps
Maximum steps	3e5 steps	1e6 steps	1e6 steps	1e6 steps
Actor network	(64, 64)	(64, 64)	(64, 64)	(256, 256)
Critic network	(64, 64, 16)	(256, 256, 16)	(64, 64, 16)	(256, 256, 128)

Table 5: Hyper-parameters of robotic environments

Hyper-parameters	Minitaur-cost	Spacereach-cost	Spacerandom-cost	Spacedualarm-cost
State shape	27	18	18	54
Action shape	8	6	6	12
Length of an episode	500 steps	200 steps	200 steps	200 steps
Maximum steps	1e6 steps	3e5 steps	5e5 steps	5e5 steps
Actor network	(256, 256)	(256, 256)	(256, 256)	(512, 512)
Critic network	(256, 256, 16)	(256, 256, 128)	(256, 256, 128)	(512, 512, 256)

589 velocities of joints, the position of the end-effector, and the position of the reference point. Then,
 590 the agent outputs the desired velocities of joints. In low-level planning, a PD controller converts
 591 the desired velocities into torques to control the manipulator. The cost function is defined as $c = d$,
 592 where d is the distance between goal and end-effector. The other settings can be found in Table 5.

593 **Spacedualarm-cost** This task aims to make a free-floating dual-arm space robot’s end-effectors
 594 reach random goal positions. The complexity of the task increases dramatically due to two arms’
 595 coupling effects on the base. The agent can obtain the state, including the angular positions and
 596 velocities of joints, the positions of end-effectors, and the position of target points of two manipulators.
 597 Then, the agent outputs the desired velocities of joints. In low-level planning, a PD controller converts
 598 the desired velocities into torques to control the manipulators. The cost function is defined as follows:
 599 $c = d_0 + d_1$, where d_i is the distance between goal and end-effector of Arm- i . The other settings can
 600 be found in Table 5.

601 E.2 Implementation Details

602 E.2.1 Baselines

603 **SAC-cost** Soft Actor-Critic (SAC) is an off-policy maximum entropy actor-critic algorithm [18].
 604 The main contribution is to add a maximum entropy objective into standard algorithms. The soft Q
 605 and V functions are trained to minimize the soft Bellman residual, and the policy can be learned by
 606 directly minimizing the expected KL-divergence. The only difference between SAC and SAC-cost is
 607 replacing maximizing a reward function with minimizing a cost function. The hyper-parameters of
 608 **SAC-cost** is illustrated in Table 6.

Table 6: Hyper-parameters of SAC-cost

Hyper-parameters	SAC-cost
Learning rate of actor	1.e-4
Learning rate of critic	3.e-4
Optimizer	Adam
ReplayBuffer size	10^6
Discount (γ)	0.995
Polyak ($1 - \tau$)	0.995
Entropy coefficient	1
Batch size	256

609 **SPPO** Safe proximal policy optimization (SPPO) is a Lyapunov-based safe policy optimization
 610 algorithm. The neural Lyapunov network is constructed to prevent unsafe behaviors. Actually, the
 611 safe projection method is inspired by the TRPO algorithm [42]. In this paper, we modify it to apply
 612 the Lyapunov constraints on the MDP tasks, similar to the process in [9]. The hyper-parameters of
 613 **SPPO** is illustrated in Table 7.

Table 7: Hyper-parameters of **SPPO**

Hyper-parameters	SPPO
Learning rate of actor	1.e-4
Learning rate of Lyapunov	3.e-4
Optimizer	Adam
Discount (γ)	0.995
GAE parameter (λ)	0.95
Clipping range	0.2
KL constraint (δ)	0.2
Fisher estimation fraction	0.1
Conjugate gradient steps	10
Conjugate gradient damping	0.1
Backtracking steps	10
Timesteps per iteration	2000

614 **LAC** Lyapunov-based Actor-Critic(LAC) algorithm is an actor-critic RL-based algorithm jointly
 615 learning a neural controller and Lyapunov function [9]. Particularly, they propose a data-driven
 616 stability condition on the expected value over the state space. Moreover, they have found that the
 617 method achieves high generalization and robustness. The hyper-parameters of **LAC** is illustrated in
 618 Table 8. Among them, α_3 is 0.1 in **LAC**, while it is changed as 1 in **LAC***.

Table 8: Hyperparameters of **LAC**

Hyperparameters	LAC
Learning rate of actor	1.e-4
Learning rate of Lyapunov	3.e-4
Learning rate of Lorange multiplier	3.e-4
Optimizer	Adam
ReplayBuffer size	10^6
Discount (γ)	0.995
Polyak ($1 - \tau$)	0.995
Parameter of Lyapunov constraint (α_3)	0.1
Batch size	256

619 **POLYC** Policy Optimization with Self-Learned Almost Lyapunov Critics (POLYC) algorithm is
 620 built on the standard PPO algorithm [43]. Introducing a Lyapunov function without access to the cost
 621 allows the agent to self-learn the Lyapunov critic function by minimizing the Lyapunov risk. The
 622 hyper-parameters of **POLYC** is illustrated in Table 9.

623 **LBPO** Lyapunov Barrier Policy Optimization (LBPO) algorithm [16] is built on SPPO algorithm
 624 [17]. However, the core improvement uses a Lyapunov-based barrier function to restrict the policy
 625 update to a safe set for each training iteration. Compared with the SPPO algorithm, the method avoids
 626 backtracking to ensure safety. For the implementation in our paper, the process is similar to that of
 627 the SPPO algorithm. The hyperparameters of **LBPO** is illustrated in Table 10.

628 **TNLF** Twin Neural Lyapunov Function (TNLF) algorithm is proposed to deal with safe robot
 629 navigation in [11]. Different from other approaches, the TNLF method defines a Lyapunov V function
 630 and Lyapunov Q function, which are trained by minimizing the Lyapunov risk. In effect, the Lyapunov

Table 9: Hyper-parameters of **POLYC**

Hyper-parameters	POLYC
Learning rate of actor	1.e-4
Learning rate of critic	3.e-4
Learning rate of Lyapunov	3.e-4
Optimizer	Adam
Discount (γ)	0.995
GAE parameter (λ)	0.95
Weight of Lyapunov constraint (β)	0.1
Clipping range	0.2
Timesteps per iteration	2000

Table 10: Hyperparameters of **LBPO**

Hyperparameters	LBPO
Learning rate of actor	1.e-4
Learning rate of critic	1.e-4
Learning rate of Lyapunov	3.e-4
Optimizer	Adam
Discount (γ)	0.99
GAE parameter (λ)	0.97
Clipping range	0.2
KL constraint	0.012
Fisher estimation fraction	0.1
Conjugate gradient steps	10
Conjugate gradient damping	0.1
Backtracking steps	10
Weight of Lyapunov constraint (β)	0.01
Timesteps per iteration	2000

631 risk is similar to that of [10]. Since the Lyapunov function strictly decreases over time, the robot
632 starting with any state in a Region of Attraction (RoA) will always stay in the RoA in the future. It
633 should be pointed out that as our environments only support the cost function, the objective, except
634 for Lyapunov risk, is to minimize the cumulative return of cost. The hyper-parameters of **TNLF** is
635 illustrated in Table 11.

Table 11: Hyper-parameters of **TNLF**

Hyper-parameters	TNLF
Learning rate of actor	1.e-4
Learning rate of critic	3.e-4
Learning rate of Lyapunov V functiob	3.e-4
Learning rate of Lyapunov functiob	3.e-4
Optimizer	Adam
ReplayBuffer size	10^6
Discount (γ)	0.995
Polyak ($1 - \tau$)	0.995
Weight of Lyapunov constraint (α)	0.1
Variance of noise distribution	1
Batch size	256

636 E.2.2 Our method

637 **ALAC** Our method offers a significant advantage in contrast to baselines, which is to use fewer
638 hyperparameters. The main hyperparameters are illustrated in Table 12. We notice that these
639 parameters control networks' learning without including the parameters of constraints. The reason is

640 they are automatically updated according to Lagrange multipliers, λ_l , and λ_e . The initial value of
 641 Lagrange multipliers is set to 1, common usage in previous constrained methods.

Table 12: Hyper-parameters of **ALAC**

Hyper-parameters	ALAC
Learning rate of actor	1.e-4
Learning rate of Lyapunov	3.e-4
Learning rate of Lagrange multipliers (λ_l and λ_e)	3.e-4
Optimizer	Adam
ReplayBuffer size	10^6
Discount (γ)	0.995
Polyak ($1 - \tau$)	0.995
Batch size	256

642 E.3 More Results on Comparison

643 Figure 10 shows the learning curves of the accumulated cost and constraint violations of **ALAC** and
 644 other baselines in ten environments.

645 E.4 More Results on Ablation Study

646 We provide the specific formulation of $\Delta\mathcal{L}_{\pi_\phi}^1$ and $\Delta\mathcal{L}_{\pi_\phi}^2$. Compared with $\Delta\mathcal{L}_{\pi_\phi}$ in Equation 9, we
 647 intuitively find that $\Delta\mathcal{L}_{\pi_\phi}^1$ and $\Delta\mathcal{L}_{\pi_\phi}^2$ are lower and higher bound of $\Delta\mathcal{L}_{\pi_\phi}$ respectively. In other
 648 words, $\Delta\mathcal{L}_{\pi_\phi}^1$ represents the strongest constraint, while $\Delta\mathcal{L}_{\pi_\phi}^2$ represents the loosest constraint. The
 649 comparison between them can demonstrate that the sampling-based Lyapunov stability ($\Delta\mathcal{L}_{\pi_\phi}$) can
 650 search for the optimal policy with stability guarantee due to the adaptive updating of λ .

$$\begin{aligned}
 \Delta\mathcal{L}_{\pi_\phi}^1(s, a) &= \mathcal{L}_\theta(s', \pi_\phi(\cdot|s')) - \mathcal{L}_\theta(s, a) + k[\mathcal{L}_\theta(s, a) - 0] \\
 \Delta\mathcal{L}_{\pi_\phi}^2(s, a) &= \mathcal{L}_\theta(s', \pi_\phi(\cdot|s')) - \mathcal{L}_\theta(s, a) + k[\mathcal{L}_\theta(s, a) - \mathcal{L}_\theta(s', \pi_\phi(\cdot|s'))] \\
 \Delta\mathcal{L}_{\pi_\phi}(s, a) &= \mathcal{L}_\theta(s', \pi_\phi(\cdot|s')) - \mathcal{L}_\theta(s, a) + k[\mathcal{L}_\theta(s, a) - \lambda\mathcal{L}_\theta(s', \pi_\phi(\cdot|s'))]
 \end{aligned} \tag{51}$$

651 The ablation experiments on other tasks are shown in Figure 9.

652 E.5 Details of Visualization

653 Our RL-based policy optimization method guided by adaptive stability is difficult to express the latent
 654 laws of states in the convergent process of different environments as the high-dimension states-space.
 655 To find and show the state’s change laws in the convergent process:

- 656 • We use the t-SNE dimension reduction technique to visualize the state-space.
- 657 • We plot the phase trajectory with variance according to the state pairs of joint angular
 658 position and velocity.
- 659 • We plot the Lyapunov-value surface and its shadow with the phase trajectory and values in
 660 the convergence process.

661 **T-SNE Visualization** The top row of Figure 4 shows the results of the t-SNE state plot-
 662 ting with SciKit-Learn tools(i.e.sklearn.manifold.TSNE function) with varying parameters(e.g.
 663 early_exaggeration, min_grad_norm). Cartpole-Cost is visualized with n_components=2 while
 664 other environments with n_components=3. The hyper-parameters for t-SNE are shown in Table 13.

665 **Phase Trajectories of Systems** We select the angular position and velocity of a joint in the state
 666 space in each environment and plot the phase trajectory with variance in Figure 6. The convergent
 667 process is shown as the angular velocity starts from 0 to 0, and the joint angle starts from the beginning
 668 to the convergence position.

```

1  n_components=2 or 3,
2  early_exaggeration=12,
3  learning_rate=200.0,
4  n_iter=1000,
5  n_iter_without_progress=300,
6  min_grad_norm=1e-7,
7  perplexity=30,
8  metric="euclidean",
9  n_jobs=None,
10 random_state=42,
11 verbose=True,
12 init='pca'

```

Table 13: Other hyper-parameters of t-SNE method.

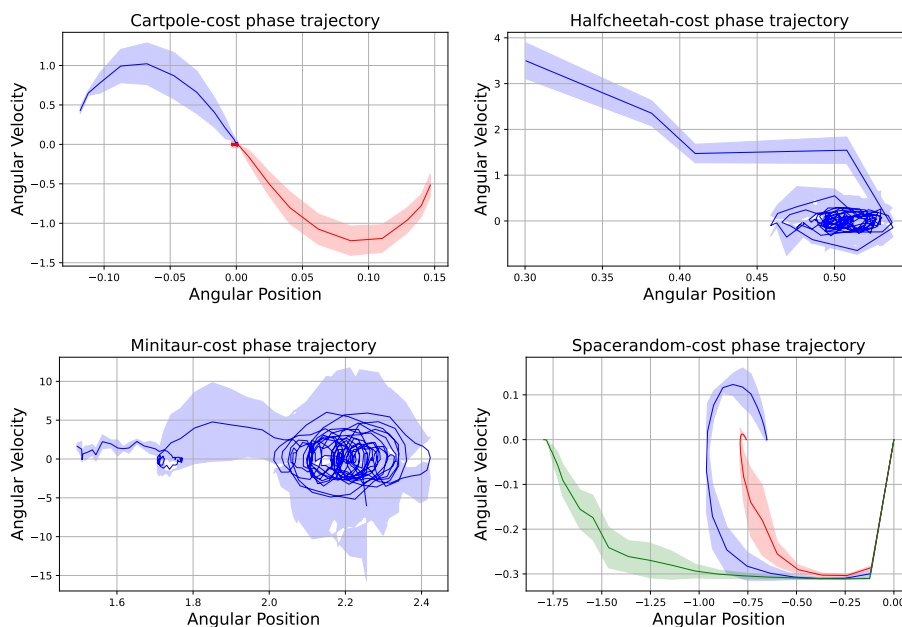


Figure 6: Phase trajectories of the systems trained by ALAC. (we report the results of 20 trials and select a joint to graph the phase trajectory in each task.)

669 **Lyapunov Functions of Systems** We visualize the change of Lyapunov-value in 3 dimensions
670 based on the phase trajectory. The second row of Figure 4 shows the Lyapunov-value surface. The
671 curves of values along the phase trajectory are mapped to the whole plane with down-sampled and
672 smoothed by a Gaussian filter; we add the values and the phase trajectory shadows correspondingly
673 simultaneously.

674 E.6 More Results on Evaluation

675 E.6.1 Robustness

676 We verify that ALAC achieves excellent robustness on most tasks. It is worth noting that we introduce
677 periodic external disturbances with different magnitudes in each task. Furthermore, we omit the
678 algorithms which do not converge to a reasonable solution in each task.

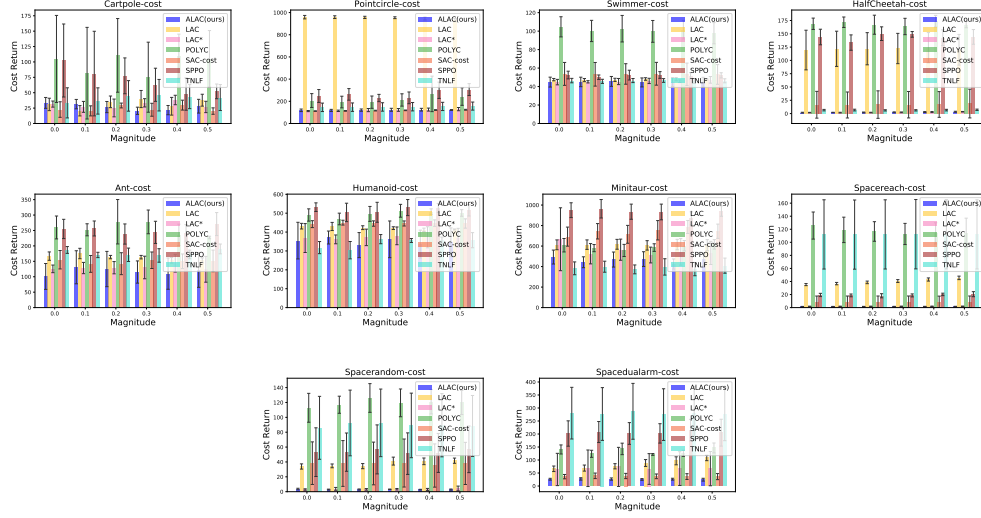


Figure 7: Performance of ALAC method and other baselines under persistent disturbances with different magnitudes. (The X-axis indicates the magnitude of the applied disturbance. We evaluate the trained policies for 20 trials in each setting.)

679 **E.6.2 Generalization**

680 We verify that **ALAC** achieves excellent generalization with the feedback of errors. In particular, the
 681 gap between each other enlarges with the increasing biases. Furthermore, we observe that the errors
 682 bring a negative impact on the performance of **SAC-cost**. The reason can be that **SAC-cost** does not
 683 capture the error information without the guidance of a Lyapunov function. Note that the number of
 684 environment steps in **Halfcheetah-cost** is $5e5$ in this section.

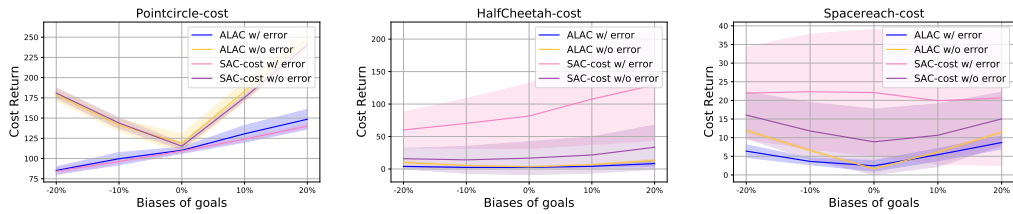


Figure 8: Evaluation of ALAC and SAC-cost methods in the presence of different biases of goals. (The X-axis indicates the magnitude of the applied shifting. We evaluate the trained policies for 20 trials in each setting.)

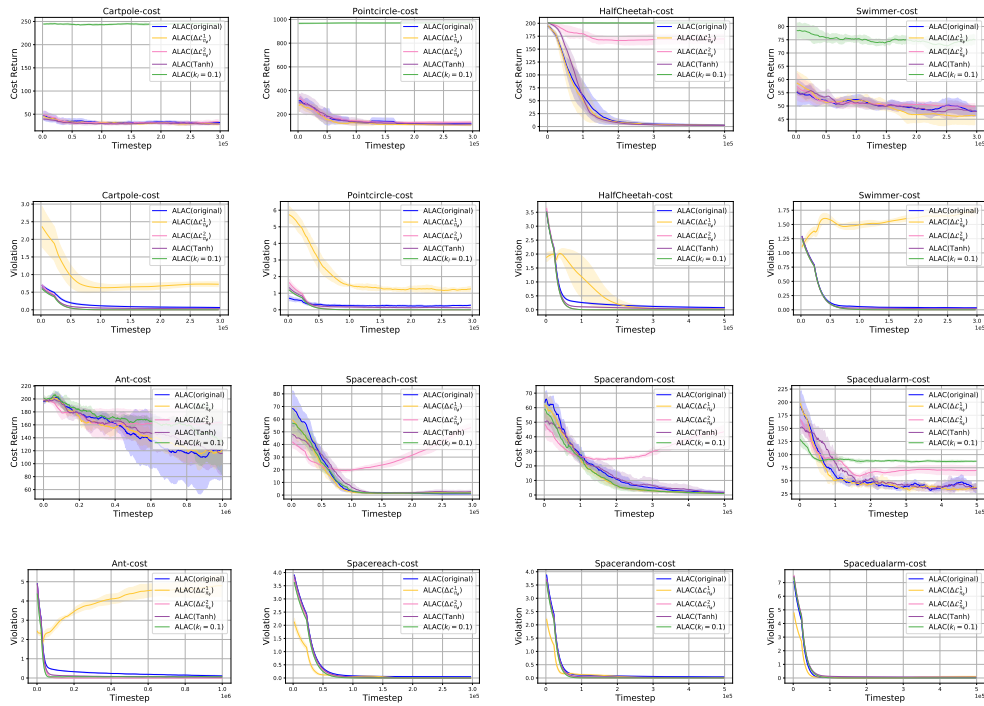


Figure 9: Ablation studies of our method. ALAC(original) shows comparable or the best performance compared with other certifications on each task.

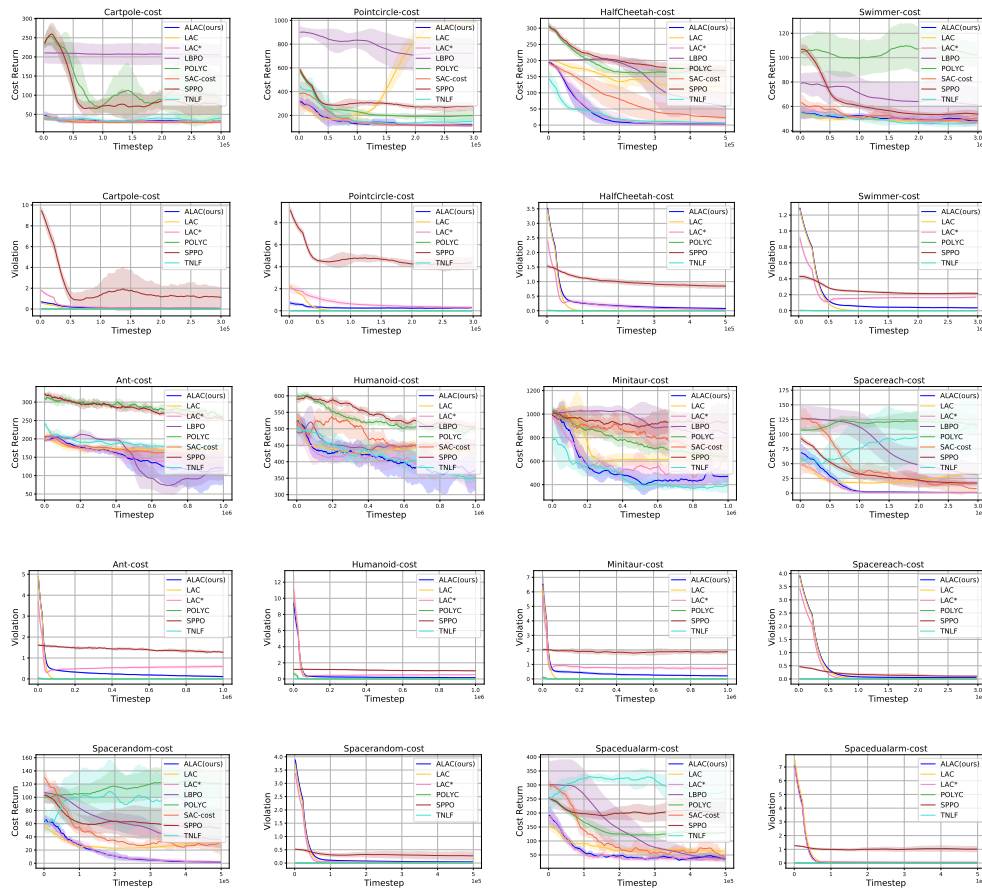


Figure 10: Performance comparison on ten tasks. The ALAC method finds a good trade-off between minimizing the accumulated cost and constraint violations in contrast to their rivals.